

Review

Remote Sensing, Geophysics, and Modeling to Support Precision Agriculture—Part 2: Irrigation Management

Arya Pradipta ^{1,*}, Pantelis Soupios ¹, Nektarios Kourgialas ^{2,*}, Maria Doula ³, Zoi Dokou ⁴,
Mohammad Makkawi ¹, Mohammed Alfarhan ⁵, Bassam Tawabini ¹, Panagiotis Kirmizakis ¹
and Mohamed Yassin ⁶

- ¹ Department of Geosciences, College of Petroleum Engineering & Geosciences, King Fahd University of Petroleum & Minerals, Dhahran 31261, Saudi Arabia; panteleimon.soupios@kfupm.edu.sa (P.S.); makkawi@kfupm.edu.sa (M.M.); bassamst@kfupm.edu.sa (B.T.); p.kirmizakis@kfupm.edu.sa (P.K.)
 - ² Lab. of Water Resources, Irrigation & Env. Geoinformatics, Institute of Olive Tree, Subtropical Plants and Viticulture, Hellenic Agricultural Organization (ELGO Dimitra), 73100 Chania, Greece
 - ³ Laboratory of Non-Parasitic Diseases, Benaki Phytopathological Institute, 14561 Athens, Greece; mdoula@otenet.gr
 - ⁴ Department of Civil and Environmental Engineering, California State University, Sacramento, CA 90032, USA; zoi.dokou@csus.edu
 - ⁵ Remote Sensing Lab, College of Petroleum Engineering & Geosciences, King Fahd University of Petroleum & Minerals, Dhahran 31261, Saudi Arabia; mohammed.alfarhan@kfupm.edu.sa
 - ⁶ Interdisciplinary Research Center for Membranes and Water Security, King Fahd University of Petroleum and Minerals, Dhahran 31261, Saudi Arabia; mohamedgadir@kfupm.edu.sa
- * Correspondence: arprdipta@gmail.com (A.P.); kourgialas@elgo.iosv.gr (N.K.)



Citation: Pradipta, A.; Soupios, P.; Kourgialas, N.; Doula, M.; Dokou, Z.; Makkawi, M.; Alfarhan, M.; Tawabini, B.; Kirmizakis, P.; Yassin, M. Remote Sensing, Geophysics, and Modeling to Support Precision Agriculture—Part 2: Irrigation Management. *Water* **2022**, *14*, 1157. <https://doi.org/10.3390/w14071157>

Academic Editor: Athanasios Loukas

Received: 27 January 2022

Accepted: 2 April 2022

Published: 4 April 2022

Publisher's Note: MDPI stays neutral with regard to jurisdictional claims in published maps and institutional affiliations.



Copyright: © 2022 by the authors. Licensee MDPI, Basel, Switzerland. This article is an open access article distributed under the terms and conditions of the Creative Commons Attribution (CC BY) license (<https://creativecommons.org/licenses/by/4.0/>).

Abstract: Food and water security are considered the most critical issues globally due to the projected population growth placing pressure on agricultural systems. Because agricultural activity is known to be the largest consumer of freshwater, the unsustainable irrigation water use required by crops to grow might lead to rapid freshwater depletion. Precision agriculture has emerged as a feasible concept to maintain farm productivity while facing future problems such as climate change, freshwater depletion, and environmental degradation. Agriculture is regarded as a complex system due to the variability of soil, crops, topography, and climate, and its interconnection with water availability and scarcity. Therefore, understanding these variables' spatial and temporal behavior is essential in order to support precision agriculture by implementing optimum irrigation water use. Nowadays, numerous cost- and time-effective methods have been highlighted and implemented in order to optimize on-farm productivity without threatening the quantity and quality of the environmental resources. Remote sensing can provide lateral distribution information for areas of interest from the regional scale to the farm scale, while geophysics can investigate non-invasively the sub-surface soil (vertically and laterally), mapping large spatial and temporal domains. Likewise, agro-hydrological modelling can overcome the insufficient on-farm physicochemical dataset which is spatially and temporally required for precision agriculture in the context of irrigation water scheduling.

Keywords: irrigation; crop growth; precision agriculture; remote sensing; agro-geophysics; modeling

1. Introduction

Because large amounts of freshwater are required to enhance crop yield, irrigation is crucial to ensure food security [1]. Globally, irrigated agriculture is responsible for around 70% of freshwater abstraction, 90% of water consumption, and 40% of food production [2]. However, the efficiency of irrigation water use is considered to be very low, as only 55% of freshwater withdrawal is consumed by the crop [3]. This unsustainable freshwater withdrawal leads to rapid surface water and groundwater depletion in many agricultural areas [4]. The challenge is more prominent in semi-arid and arid regions that are currently

under water stress and are relying on groundwater resources to support irrigation practices [5–7]. Furthermore, the expansion of global agriculture areas is expected to increase to meet the increasing demand for agricultural commodities due to population growth. Therefore, without proper irrigation water management techniques and practices, and considering the effect of climate change, freshwater preservation and future food production will be threatened.

A good understanding of the relationship between the soil water content and the plant is necessary, as the growth of the crop is governed by the water supply and demand in the soil-plant-atmosphere continuum [8]. In reality, the irrigation water requirement might vary in the field, depending on plant and soil properties and environmental status. Soil, water, and plant properties are not considered static parameters, but they constantly change over space and time [9]. Thus, the regular monitoring of soil water availability and crop growth is essential to establish precision water irrigation [10]. Moreover, the implementation of precision irrigation water would allow decision-makers and farmers to sustain limited freshwater resources while at the same time also enhancing on-farm productivity.

Nowadays, remote sensing, geophysics, and agrohydrological modeling have been widely applied as decision-making tools for site-specific irrigation water management. The use of the tools mentioned above is considered part of the innovation in precision agriculture. Dynamic processes in the soil-plant-atmosphere continuum, as well as the plant's physical properties such as soil moisture (SM), root water uptake (RWU), evapotranspiration (ET), crop chlorophyll, leaf area index (LAI) and plant water status content, could be retrieved through remote sensing or geophysical acquisition. In turn, these data could be used as inputs for agrohydrological modeling in order to provide an estimation of crop water requirements for optimal yields. That advanced information would be beneficial for the decision-making process at the farm-scale in order to achieve precision agriculture. The present paper intends to highlight applications of remote sensing, geophysics, and modeling to support proper irrigation water management. The overall concept is presented in the flowchart of Figure 1.

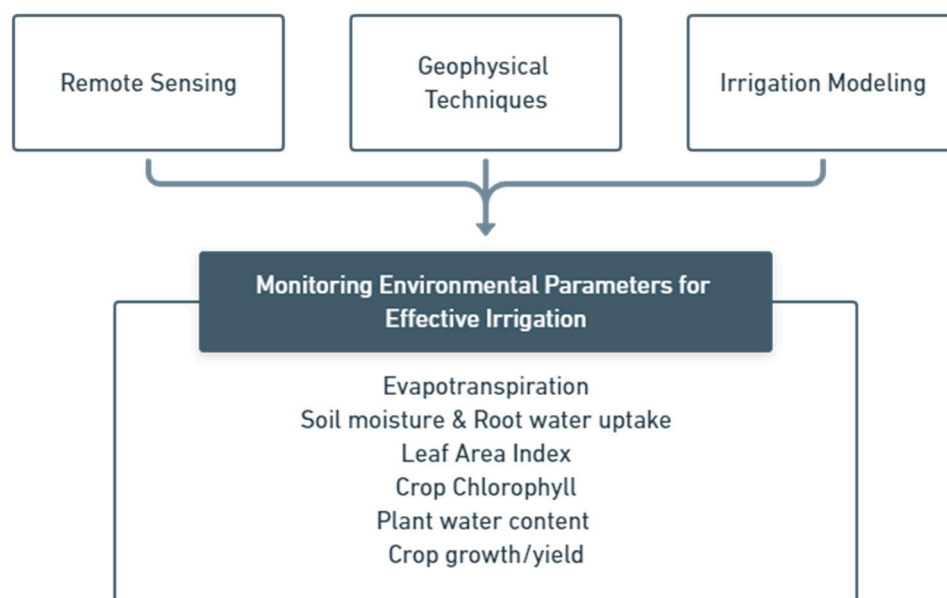


Figure 1. Flowchart of precision agricultural services to support proper irrigation management.

2. Irrigation and Crop Monitoring in Precision Agriculture

The adequate measurement of crop water requirements can be considered the first step toward implementing irrigation water efficiency. Quantifying the right amount of irrigation water supply typically involves the crop water requirement and soil water balance, where ET is the main component [11]. ET, which is a turbulent flux of water vapor from the surface

into the atmosphere involving soil evaporation and transpiration, can also be defined as the amount of water required by plants [12]. ET is regarded as the most significant outgoing water flux at the land surface, and any change of this variable will directly affect the water availability [13]. Thus, accurate knowledge of ET is crucial for a greater understanding of the water and energy balance, which is beneficial for numerous implementations such as irrigation water strategies.

Irrigation water allocation cannot be set in a uniform manner, as the biomass and soil texture might vary across the field, thus affecting the crop water requirement. Conventional techniques like lysimeter, eddy covariance, sap flow, pan measurement, and the Bowen ratio offer an accurate ET estimate at the individual crop and field scales. However, most of the aforementioned methods are difficult to extrapolate into a larger scale to identify on-farm spatial variability considering the heterogeneity of the land surface and heat transfer process. Hence, remote sensing is regarded as a suitable tool to overcome this gap due to its ability to provide adequate spatial and temporal information.

In the cultivated area, shallow soil characteristics (e.g., soil texture and structure) at a depth of 1–2 m might govern irrigation water distribution, the availability of nutrients, and root growth. Soil texture is defined as the relative proportion of gravel, sand, silt, and clay. At the same time, soil structure refers to the spatial arrangement of different solid constituents (e.g., mineral and organic matter) and the soil void. Coarser soil like sandy soil can be wetted by lesser irrigation, but it is easily dried up, resulting in frequent irrigation schedules. On the contrary, fine-textured soil is more fertile, and can hold soil water longer than coarser soil. Soil water movement and retention in the vadose zone are also influenced by the soil structure. Poor soil structure, such as soil with low permeability, could reduce the irrigation water infiltration and increase runoff. This characteristic might result from the compaction process due to the heavy equipment used in agricultural activity. Because these soil characteristics are not homogeneous within farm areas, they might affect the irrigation water management plan. Therefore, an accurate assessment of the subsurface soil at the field scale is required in order to support precision irrigation.

Other variables required for precision irrigation are the hydrological state and flux in the vadose zone, such as SM and RWU. Both variables are affected by each other; thus, understanding the spatiotemporal variability of SM and RWU would be beneficial to support decision making regarding the optimum irrigation scheme [14–16]. SM refers to the amount of water in the soil, and is commonly expressed as a percentage. SM is the essential variable influencing the transfer of energy, carbon, and water in the soil-plant-atmosphere continuum. In agricultural areas, a sufficient amount of SM is required by a crop to grow. This variable can be quantified through numerous approaches at various scales, from the point scale to the local and/or regional scale. The most traditional method is probably the application of gravimetric and volumetric soil water content equations after performing soil sampling. Another reliable technique at the point scale is the deployment of several electromagnetic sensors, such as time domain reflectometry (TDR), amplitude domain reflectometry (AWR), and frequent domain reflectometry (FDR) inside the soil to measure the volumetric water content [17]. At the proximal scale, several geophysics techniques can be employed, such as resistivity [18,19], ground-penetrating radar (GPR) [20], or electromagnetic induction (EMI) [17]. Nowadays, remote sensing approaches have been successfully proven to monitor surface soil moisture (SSM) at different scales. On the other hand, RWU is defined as the process of water extraction by plant roots for transpiration. In particular, the assessment of RWU is based on the adequate information of SM. The study of RWU typically focuses on the determination of the area where the water is extracted by plant roots, and the analysis of the major factor affecting RWU, such as changes of water availability or salinity [16].

Crop monitoring is one of the activities in precision agriculture that is commonly oriented towards retrieving key parameters such as the Leaf Area Index (LAI), chlorophyll content (e.g., leaf and canopy), and plant water status. Based on these three parameters, early agricultural yield can be calculated to affect farm planning and decision-making.

Water and nutrient supplies that vary in space and time are considered the most important variables influencing crop productivity [9]. Besides LAI and chlorophyll, several factors like pest, insect, and disease monitoring should be considered, as they could have adverse effects on crop development, such as yield reduction. The earlier these adverse factors can be identified, the easier the problem will be to address. Therefore, by implementing effective crop monitoring, the risk of economic loss can be potentially reduced.

Measuring leaf chlorophyll content, which is an indicator of photosynthesis and a principal parameter of crop productivity, could assist farmers in defining leaf nitrogen content. Among nutrients, nitrogen is regarded as the most important for crop productivity. Therefore, farmers should make an effort to balance the nitrogen supply to the crop's needs. Apart from increasing farm management costs, excess nitrogen supply could result in soil overloading, leaching or run-off and eutrophication to water bodies, causing soil and water degradation. On the other hand, a deficiency of the nitrogen supply might reduce the agricultural yield [21,22]. The early crop growth stage is a crucial period within the cultivation cycle, as it affects crop yield; thus, a sufficient rate of nitrogen to be applied across the field should be adequately determined [21].

The leaf chlorophyll concentration can be quantified through in situ measurements [23] or using remotely sensed observations [21,24,25]. The conventional and most accurate technique is chlorophyll extraction using organic solvent extraction and supercritical fluid extraction [26]. As a recent development, optical sensors offer a rapid, non-destructive, inexpensive technique to quantify leaf chlorophyll content through reflectance measurement [21,27,28]. The latter method has been widely applied due to its advantages, and can be adopted by in situ or remotely sensed observation. In addition, remote sensing provides opportunities in precision agriculture that require the scaling-up of the individual data from the plant level to the field level, as it could cover large monitoring areas. Through this approach, leaf chlorophyll is multiplied with LAI to obtain the total chlorophyll concentration per ground area [27,29,30]. However, the measurement of chlorophyll content by remote sensing at a large scale can be challenging, as the canopy reflectance is affected by structural factors that might mask the reflectance, such as canopy architecture, chlorophyll distribution, LAI, or soil background [27,31]. Thus, the acquired leaf reflectance within the same canopy might differ even for the same chlorophyll content [32].

Another critical index that reflects the biochemical and physiological process of vegetation, indicating plant productivity, is LAI [33,34]. This dimensionless variable is described as the leaf area ratio per unit of ground surface area [35]. The green leaf area is highly influenced by nitrogen, temperature, and water. Therefore, LAI measurement would be an effective method to understand crop responses to the implemented irrigation scheme. The leaf is also a medium in which photosynthesis takes place. Considering that the photosynthesis process governs crop production, LAI can be used for fertilization management, pruning, and spraying, and to predict crop growth and yield [36–38]. Given the importance of LAI for precision agriculture, new methods of LAI monitoring are emerging over the years. Remotely sensed observation can overcome the limitation of ground-based measurement that might be destructive and time-consuming. However, this approach still requires validation and calibration. In general, remote sensing observation for LAI measurement involves both satellites and unmanned aerial vehicles (UAVs).

Lastly, the quantitative measurement of the vegetation water content (VWC) is also necessary for crop yield estimation and precision irrigation. The VWC represents the total volume of water in the stem and canopy [39]. Basically, the canopy water content (CWC) is the product of the leaf water content (LWC) and LAI [39]. In other words, LWC and CWC can be defined as the water mass per leaf unit of area, and water mass of vegetation per unit of ground area, respectively [40]. LWC also can be referred to as the equivalent water thickness (EWT). Similarly to crop chlorophyll and LAI measurements, the remote sensing of VWC has recently become a popular method due to its rapid monitoring, time-efficiency, and cost-effectiveness.

3. Remote Sensing to Support Precision Agriculture in Irrigation Management

Many areas dedicated to crop production do not have sufficient field hydrological observations to support precision agriculture. Moreover, the field data commonly have different record lengths, and they are spatially limited, making agricultural monitoring more challenging. Due to the unprecedented development of earth science monitoring technology, remote sensing can address this issue by involving spaceborne and airborne observations. Unlike ground measurements, remote sensing has the advantages of regular spatial and temporal resolutions. Spaceborne or satellite data typically have a variety of spatial resolutions with consistent time acquisition, depending on the sensor. They can be used to observe areas of interest from the regional scale to the farm scale [41]. One of the airborne observations, UAV, offers better spatial resolution and can perform in smaller areas. Moreover, the acquisition time depends on the user, and could not be consistent with the satellite observation. For precision agriculture, the spatial resolution range should be from 0.1 m to 10 m, and the temporal resolution should be at least a few days [30,42].

3.1. Evapotranspiration

In particular, the quantification of ET through remote sensing involves numerous approaches, including the surface energy balance (SEB), vegetation index–surface temperature (VI-Ts), and water balance methods [43]. The SEB model calculates ET as a residual of the surface energy budget equation, and considers that the amount of energy entering the earth is equal to the amount of energy emerging from it [44]. This model is based on the principle of energy conservation to partition net radiation at the surface into ground heat, sensible heat, and latent heat flux, where the latter variable is referred to as the ET process [44–46].

SEB can be divided into single-source or two-source models [47]. A number of single-source SEB algorithms were developed to calculate ET through remote sensing, including the widely used model such as the Surface Energy Balance Algorithm for Land (SEBAL) [48], Mapping Evapotranspiration at High Resolution using Internalized Calibration (METRIC) [49], the Surface Energy Balanced System (SEBS) [45], and the Surface Temperature Initiated Closure (STIC) [50]. Single-source SEB models are relatively easy to perform, as they do not treat soil and vegetation as different components. However, the applications of single-source SEB models have limitations over a diverse range of surface conditions [47].

The basic principle of the two-source models is to quantify the contributions of both soil and vegetation components (evaporation and plant transpiration) to the total heat flux [51]. Moreover, the two-source models have been found to be practical to be applied, as they do not require prior calibration and additional input data from ground-based observations [44,47,52]. This is particularly useful for agricultural applications, as evaporation and transpiration are required to design proper irrigation management. The atmosphere land exchange inverse (ALEXI) [53], the Disaggregated Atmosphere Land Exchange Inverse Model (DisALEXI) [54], and the two-source energy balance model (TSEB) [51] are some representatives of the popular two-source SEB models. However, some conditions—such as fractional vegetation cover and soil water availability—might limit the accuracy of these models. In order to overcome this, several models based on two-source approaches have been developed lately, including the Soil Plant Atmosphere and Remote Sensing Evapotranspiration (SPARSE) [55], the Thermal-Based Two-Source Energy Balance for Different Seasons (TSEB-2S) [56], and the End-Member-Based Soil and Vegetation Energy Partitioning (ESVEP) [57]. SPARSE was designed to monitor ET in water-scarce environments, while TSEB-2S is practical to be implemented in a tree-grass ecosystem such as the savanna [55,56]. Lastly, ESVEP has the ability to separate the response of the SM at the upper layer to evaporation and at the deeper root zone to plant transpiration [57].

The input of SEB can be obtained from visible, near-infrared, and thermal infrared remote sensing bands ranging from the land surface temperature to albedo and VI [45,48]. These variables are then combined with ground-based meteorological data such as the air temperature, wind speed, and other near-surface variables to retrieve the net radiation, ground heat, and sensible heat flux [47]. Different satellite platforms have demonstrated

their capability to retrieve the required data for SEB input, including the Moderate Resolution Imaging Spectroradiometer (MODIS) [58–60] and Landsat [46,61,62] data. The uses of microwave sensors were also highlighted by several studies in order to overcome the major obstacle of visible, near-infrared, and thermal infrared remote sensing, which is a cloud cover. For instance, Bastiansseen et al. [63] and Mostafa et al. [64] utilized passive microwave remote sensing to retrieve SSM in order to estimate the soil evaporation in the two-source SEB models.

The VI-Ts triangle method is based on the vegetation index and land surface temperature (LST), which can be obtained from remote sensing. The VI-Ts method plots scatterplots of LST versus VI, forming triangular shape with a dry edge and a wet edge to estimate evaporative fraction (EF) and ET [65]. The wet edge is defined by the linear interpolation of pixels with minimum VI and maximum LST, while the dry edge is identified by an opposite response [43]. The VI-Ts approach is less complex, as it does not require a surface, meteorological, or land surface model as an ancillary dataset [58,66].

In order to obtain the best result of the VI-Ts method, the contrast variations of the land surface temperature and vegetation index are required; therefore, this method might not perform well in any areas characterized by a homogeneous land surface, such as desert or a rainfed agriculture area during the dry season [47,67]. Another factor restricting this method is atmospheric conditions, such as cloudiness, that can discontinue the LST retrieval [68]. Because temporally continuous ET is crucial for water resource management, previous studies have developed various techniques to address this issue. These techniques vary from the universal triangle method that transforms the VI-T feature space from the regional scale into the pixel scale [67], a gap-filling algorithm using a deep neural network (DNN) [69], and the fusion of a VI-Ts model and the LST construction method [68].

Another approach is the water balance method, which is quite simple in theory. This method estimates ET by quantifying it as a residual component using the water balance equation. The value of the ET can be obtained by subtracting the runoff (R) and change of water mass storage (ΔS) from precipitation (P) [70]. Currently, ΔS is only available from the Gravity Recovery and Climate Experiment (GRACE) satellite retrieval, which has coarser spatial resolution and suffers from periodic data gaps, thus limiting its use to the basin scale, and only with low temporal resolution [70–72]. In order to implement the water balance method in sub-basin-scale or smaller areas, further attempts commonly focused on improving the spatial resolution of GRACE through the downscaling process. For instance, Wan et al. [73] highlighted the use of the land surface model to downscale GRACE data for monthly ET monitoring in sub-basins across the United States. Yin et al. [74] explored the potential of statistical downscaling using numerous observations over a long period in order to apply the water balance method in the North China Plain. A brief overview of different remote sensing-based methods and products used to support irrigation water management is provided in Table 1.

Table 1. Brief overview of different remote sensing-based methods and products to estimate ET over irrigated areas.

Methods	Remote Sensing Platforms	Applications	References
Single-Sources Surface Energy Balance (SEBAL)	Lansat 8	Estimation of irrigated wheat requirement in the Ein Khosh Plain	[75]
Single-Sources Surface Energy Balance (STIC)	MODIS	ET mapping in the conterminous US	[76]
Two-Sources Surface Energy Balance (TSEB)	ASTER SPOT	Monitoring crop water consumption over the irrigated area of Tensift Basin	[77]
Two-Sources Surface Energy Balance (ETLook)	AMSR-E MODIS	ET mapping over irrigated area in the Indus Basin	[63]
Two-Sources Surface Energy Balance (SPARSE)	MODIS	Estimation of ET and water stress over several crop types and climates	[78]
VI-Ts triangle method	MODIS	ET estimation in the Haihe River Basin	[79]
Water balance method	GRACE	Detection of irrigation-induced ET in the Haihe River Basin	[80]

3.2. Soil Moisture

Commonly, the retrieval of SM through remote sensing mainly focuses on the use of microwave sensors, as they are strongly associated with the SM content [81,82]. At a large scale, passive microwave satellite observations such as AMSR, SMOS, and SMAP have been widely optimized and proven for their reliability to monitor SM variabilities in the top few centimeters (approximately 0–5 cm), i.e., referring to surface soil moisture (SSM) [83–86]. Recent studies have shown that SSM could serve as a basis to identify the spatial extent of irrigated regions [87,88], and to quantify the amount of water used for irrigation [89–92]. In addition to passive microwave remote sensing, active microwave satellites like Sentinel-1, RADARSAT-2, PALSAR/ALOS-2 and TerraSAR-X have feasibility for SM mapping [93–96]. Compared to passive microwave sensors, active microwave sensors offer a high spatial resolution. Hence, they can provide meaningful information at the farm scale. In contrast, passive microwave sensors would be helpful for agricultural decision-making at the local or regional scale. In terms of temporal resolution, the passive microwave has a higher revisit frequency compared to the active microwave. Both passive and active microwaves are sensitive to the soil-water dielectric constant that affects the emissivity and backscattering of microwaves, allowing them to measure SSM [97,98].

One of the limitations of spaceborne remote sensing is that it cannot capture the dynamic of SM in the deeper soil zone (root zone soil moisture (RZSM)). In cultivated areas, the information of the RZSM is important and required in order to have a meaningful impact for different applications, such as root water uptake (RWU) and soil hydraulic parameters [99]. Moreover, the ability of RZSM to reflect the actual soil water availability required by the crop is better than that of SSM [100]. In order to overcome this issue, several studies incorporated SM retrievals derived from passive microwave remote sensing into land surface or hydrological models through data assimilation schemes in order to predict RZSM [100–103]. Data assimilation is considered the most promising technique due to its ability to develop RZSM while quantifying uncertainties from observation data and output simulation [102].

Several factors, such as vegetation cover and soil characteristics, could influence the accuracy of SM retrieval. Sensor sensitivity tends to decrease with increasing vegetation density. Therefore, microwave sensors have better accuracy in areas characterized by sparse to moderate vegetation than densely vegetated areas [104]. In general, this issue can be minimized by using a longer wavelength. Among the existing passive microwave satellites, SMOS and SMAP have been widely used recently due to their L-band operation, which has the capability of penetrating vegetation cover, unlike the C-band [105–107]. Even though it is challenging, separating the effect of vegetation and soil characteristics such as soil roughness from SM would provide better accuracy, particularly for active microwave sensors, as these factors heavily perturb its backscattering. This is especially relevant at the farm or field scale, where precise irrigation management for a specific condition is necessary. In the past few years, the removal of the effect of the vegetation canopy over different crops and phenological periods through numerous methods has shown promising results, and is now feasible to be applied [94,108].

Alternative approaches to the assessment of SM are optical and thermal infrared satellite observations. Optical and thermal satellites are well-suited for small-scale observations because of their higher spatial resolutions. However, the applications of optical and thermal sensors solely for SM monitoring are still limited. The combination of both sensors (optical–thermal), known as the temperature–vegetation triangle approach, is more popular and widely used. The basic principle of the triangle approach is that SM is closely associated with the land surface temperature and vegetation index; thus, variations of SM can be estimated [109]. The visible (VIS), near- (NIR), and shortwave infrared (SWIR) bands emitted from the optical sensor can detect various plant parameters, such as greenness, canopy water, or photosynthetic parameters that related to plant water. In contrast, thermal infrared (TIR) wavebands are closely associated with soil thermal properties [110]. Numer-

ous studies have also exhibited the feasibility of combining optical and thermal sensors to determine SM variabilities [111–114].

Lately, the utilization of UAVs has become popular as part of modern agricultural management. Like satellite-based monitoring, UAV is a timesaving, non-destructive method, offers better spatial resolution, and supports real-time farm management. Wu et al. [115] demonstrated that SM could be observed by mounting ground-penetrating radar on UAVs. Another technique is the installation of optical and thermal sensors on UAVs [116,117]. Like satellites, these sensors capture vegetation index and land surface temperature information, which allow SM estimation. The overview of numerous remote sensing products for the retrieval of SSM and RZSM is depicted by Table 2.

Table 2. Overview of numerous remote sensing products and sensor types for the estimation of SSM and RZSM.

Applications	Remote Sensing Products	Sensor Types	References
Surface Soil Moisture	SMAP_SM	Microwave	[84]
	SMOS_SSM	Microwave	[85]
	AMSR2_SM	Microwave	[118]
	Sentinel-1, Sentinel-2	Microwave-Optical	[119]
	Sentinel-1 Landsat-8 OLI & TIRS	Microwave-Optical-Thermal	[93,120]
	Sentinel-2 Landsat-8 OLI & TIRS	Optical-Thermal	[114]
	MODIS_LST MODIS_Surface Reflectance	Optical-Thermal	[111]
	UAV	Optical-Thermal	[116,117]
Root Zone Soil Moisture	SMAP_SM SMOS_SSM SMOS_RZSM MODIS_LST MODIS_Surface Reflectance	Microwave-Optical	[100]
	AMSR-E_SSM MODIS_ET	Microwave-Optical	[103]

3.3. Crop Chlorophyll and LAI

Optical remote sensing in the VIS, NIR and SWIR spectra is widely used to estimate LAI and crop chlorophyll content [24,29,34,121,122]. Different materials and objects can be differentiated based on their spectral signature. Based on the number of spectral bands, optical remote sensing can be classified into several imaging systems, of which multispectral and hyperspectral sensors are the most used imaging sensors. Besides optical remote sensing, the potential of microwave remote sensing to retrieve LAI and crop chlorophyll was also explored by Clevers et al. [30]. Basically, multispectral and hyperspectral bands work by recording the electromagnetic energy reflected or emitted from the earth's surface in three to ten bands and more than ten bands, respectively. Compared to multispectral sensing, the utilization of the hyperspectral remote sensing has been increasing over the years due to its ability to provide continuous spectral coverage despite requiring more complex technical procedures [34]. However, both imageries can only provide satisfactory spatial resolution in clear atmospheric conditions.

Commonly, the estimation of the chlorophyll content and LAI relied on the empirical (statistical) spectral vegetation indices or the inversion of the radiative transfer model [123–126]. Empirical spectral vegetation indices are the simplest and most popular method that utilizes a statistical approach to determine the correlation between the observed object and vegetation indices or spectral reflectance [123,124]. However, the

complex internal and external factors affecting spectral reflectance might vary in time and space; thus, the relationship between the observed objects with their reflectance might be inadequate over heterogeneous conditions [127]. On the other hand, the inversion of a radiative model can explain the interaction of the radiation that occurred inside the canopy using physical laws; thus, the connection between the biophysical variables and canopy reflectance can be described [125]. The major limitation is that the radiative transfer model requires insitu-specific information that is not always available [24].

The quantitative estimates of some ecophysiological variables (e.g., leaf chlorophyll and LAI) are assessed using spectral reflectance in the VIS, NIR and SWIR domains. This is because leaf spectral reflectance is assumed to be related to pigment compositions, such as chlorophyll, carotenoids, and anthocyanins [28,128]. These spectral domains are then utilized to develop numerous vegetation indices (VI) to estimate the plant's biophysical parameters, including LAI. Among the developed VI, the normalized difference vegetation index (NDVI) is the most popular one. NDVI is also the VI which is least affected by soil background, and it has good accuracy, meaning that this index can be considered to be a reliable tool [31,129]. The most effective spectral reflectances used for LAI estimation are located in the NIR and SWIR regions, particularly at the wavelength of 820 nm, 1040 nm, 1200 nm, 1250 nm, 1650 nm, 2100 nm, and 2260 nm [130].

For the leaf chlorophyll estimation, Gitelson et al. [131] reported that the band wavelengths of 520 nm to 550 nm and 695 nm to 705 nm are closely related to the chlorophyll content in all of the leaf species. A similar range of absorption features has also been mentioned by Delagido et al. [29] and Daughtry et al. [132], for whom chlorophyll concentrations are related to the wavelengths of 643 nm to 795 nm and 550 nm and 715 nm, respectively. Based on these results, it can be concluded that leaf chlorophyll has strong absorption in the VIS and NIR domains.

3.4. Vegetation Water Content

VWC quantification through remote sensing generally assesses several vegetation physiological indicators, such as stomatal conductance, leaf water potential, canopy water content, leaf equivalent water thickness, live fuel moisture content, and relative water content [133]. Basically, optical and microwave remote sensing are the two common approaches which are utilized in VWC measurement (Table 3). Besides them, the use of thermal remote sensing was also explored by several studies.

Optical remote sensing can be considered as the conventional approach to measure VWC. The volume of water in vegetation commonly has strong absorption features in the NIR and SWIR spectral regions, thus allowing us to quantify VWC [130,134,135]. For example, Ullah et al. [134] mentioned that spectral reflectances of 1397 nm and 1600 nm are related to LWC, while Jin et al. [135] identified 75 wavelengths related to LWC, with a range from 926 nm to 1940 nm. The use of NIR or SWIR solely is not suitable to retrieve VWC, particularly at the leaf level (LWC); thus their combination is required [136]. Therefore, different vegetation indices based on spectral reflectance have been utilized to assess VWC, such as the normalized difference infrared index (NDII), the normalized difference vegetation index (NDVI), the normalized difference water index (NDWI), and the canopy temperature [137]. Among these indices, NDWI that employs NIR and SWIR provides a better estimate of VWC, as reported by previous studies [138,139].

Recently, active microwave remote sensing or radar have been carried out by a number of studies to retrieve VWC. One radar-based vegetation index to monitor crop properties, named the radar vegetation index (RVI) was developed and applied for VWC measurement [140–142]. This index represents a simple function of radar backscattered from all polarizations, including co- and cross-polarization [142]. RVI is not only applied to assess VWC, but also the vegetation greenness and LAI. Technically, the reduction of VWC will be reflected by the decreasing RVI from the L-, C-, and X-bands [141]. The L-band has been found to have better accuracy for VWC retrieval compared to the C- and X-bands due to its better penetration [141,143].

One of the limitations of RVI is the sensitivity of radar measurement to soil scattering (moisture and roughness). Therefore, the revised RVIs named RVII and RVIII were proposed by Szigarski et al. [144] to reduce the effect of soil moisture and roughness. Besides RVI and RVII, other radar-based vegetation indices were also developed to improve their performance in VWC measurement, e.g., the polarimetric radar vegetation index (PRVI) that exploits the polarization degree and the cross-polarized backscattering coefficient [145], and the dual polarimetric radar vegetation index (DpRVI) [146]. The latter index utilizes the normalized dominant eigenvalue and the degree of polarization instead of polarization backscatter intensities [146].

Several findings showed that thermal infrared (TIR) remote sensing can be utilized to retrieve VWC, particularly at the leaf level. Despite its potential, the use of TIR in VWC has not been heavily exploited due to several reasons. The relationship between VWC and spectral features in the TIR domain is relatively weak compared to the NIR and SWIR regions [147]. Regarding the spaceborne platform, the number of TIR satellites is still limited to a few satellites—for instance MODIS, Landsat-8 and Sentinel-3—thus limiting its use at a larger scale [148]. An additional issue restricting the use of TIR satellites in VWC studies is the scaling process from the leaf to the canopy level [149].

Table 3. A number of remote sensing platforms and sensor types in crop development monitoring.

Applications	Platforms	Sensor Types	References
Crop chlorophyll content	PROBA	Optical	[29,150]
	UAV	Optical-Thermal	[24]
	UAV	Optical	[122,151]
LAI	Sentinel-2	Optical	[30]
	Compact Airborne Spectrographic Imager	Optical	[121]
	UAV	Optical	[122,151]
VWC	Sentinel-2	Optical	[152]
	Lansat 5, ASTER, and AWiFS	Optical	[153]
	MODIS	Optical	[139]
	Sentinel-1	Microwave	[146]
	SMAP	Microwave	[142]

4. Geophysical Acquisitions

Potential agricultural geophysical applications are widespread, varying from soil structure characterization to SM assessment. Geophysical acquisitions are regarded as non-invasive, non-destructive, rapid, and cost-effective methods that are frequently used for soil investigation. Those methods would allow the user to investigate all of the sub-surface soil without disturbing the structure and dynamic of the soil [154]. In addition, the geophysical survey can map large spatial and temporal domains, bridging the gap between remote sensing observations and point-based measurements. Moreover, information derived from the geophysical survey could also be utilized to calibrate or validate remote sensing measurement.

Basically, resistivity, EMI, and GPR are the most common geophysical methods employed for agricultural applications [155]. Soil properties and state variables such as porosity, density, clay content, SM, and salinity are the typical parameters observed through a geophysical survey [156]. Besides them, magnetometry, self-potential, and seismic methods are three promising geophysical methods that can be applied for the same purpose in the future [155]. However, the interpretation phase in geophysics poses a challenge for the

user due to its ambiguity. Therefore, the combination of different available geophysical methods and the integration of the final geophysical model with other parameters such as geochemical and remote sensing in datalogs are usually applied to minimize uncertainties and improve the final geophysical solution. Table 4 provides an overview of different applications of geophysical methods used to assess the soil water availability and dynamic in the vadose zone.

4.1. Soil Characteristics

Subsurface soil characterization is considered to be a prerequisite step of agricultural management. Several soil parameters—such as soil texture and structure—that might govern the distribution of water irrigation can be potentially monitored using geophysics-based assessment. Some geophysical methods like resistivity and seismic assessment are expected to have strong soil texture and structure signatures.

The feasibility of electrical resistivity (ER) to identify a tilled soil structure in the agricultural area has been examined by several studies. ER is known to be sensitive to bulk density, where increasing bulk density due to soil compaction corresponds to a reduction of porosity, air and pore water volume, an increase of clay fraction, and subsequently the decrease of the soil ER [157–160]. However, the degree of compaction cannot be directly measured by ER [161]. As an extension of ER, electrical resistivity tomography (ERT) can develop a high resolution of the 3D subsurface soil structure that enables a user to investigate soil facies based on the seasonal soil water content period [162,163]. Other applications of ERT for soil characterization include, but are not limited to, soil compaction [164], the soil–rock interface [165], and soil organic matter (SOM) delineation [166–171].

The soil's apparent electrical conductivity (ECa), measured by EMI, can indirectly indicate several soil properties that influence agricultural productivity [172,173]. In the irrigated landscape, EMI is becoming one of the frequently used approaches to map the subsurface due to its high mobility. Subsurface soil characterization through EMI can be acquired faster than other instruments, as the induction principle of EMI does not require direct contact with the ground surface [174]. Confounding geophysical interpretation might appear as a combination of various soil properties, which could affect ECa. Some approaches have been proposed and established in order to overcome this issue, involving simple statistical correlations and wavelet analysis [172]. Soil texture assessment through EMI generally focuses on the clay content, rather than sand and silt compositions [175–178], while soil structure evaluation typically pays more attention to reduced permeability due to soil compaction [179,180].

While ERT and EMI offer a general spatial pattern of the soil, GPR has the ability to provide detailed information on soil stratigraphy [181]. The antenna frequencies should be appropriately selected based on the aim of acquisition and field conditions [182]. In the agricultural field, one of the exciting aspects of the GPR applications is soil structure monitoring based on dielectric permittivity, as this would affect water movement within the vadose zone [183–185]. Another application for soil characterization assessment required in agricultural studies is compacted layer assessment [186,187]. Basically, the effectiveness of GPR in soil assessment is related to the soil condition. For example, the implementation of GPR in soil dominated by clay is difficult due to the strong absorption of radar waves.

Even though the use of seismic assessment in soil studies is still rare, the sensitivity of the shallow seismic method offers better soil mechanical measurements such as compacted layers and aggregation than other geophysical techniques [156,188]. This method analyses the propagation velocity of the seismic wave, which is affected by material properties. Soil compaction will result in an increase of bulk density; subsequently, the velocity of the seismic wave will increase as well [159]. Several studies have also identified a significant difference in seismic wave velocities representing compact and loose soil [189,190].

4.2. Soil Water Availability and Dynamic

High-resolution SM mapping in 2D and 3D models commonly employs resistivity [191–194], EMI [195–197] and GPR [196,198,199]. These geophysical techniques might

overcome the scale gap between point-scale SM sensors, such as time-domain reflectometry (TDR) sensors and remote sensing observation [17,200]. Moreover, information on SM derived by the geophysical technique is generally used as a basis to characterize the spatiotemporality of RWU [16].

ERT is one of the most appropriate methods to monitor the spatiotemporal resolution of SM at the field scale by measuring the bulk soil electrical conductivity. It is widely known that the variability of soil electrical resistivity is highly affected by the soil water content [158,191], allowing a user to determine SM variabilities. In order to convert the bulk soil electrical conductivity into the soil water content, the in situ calibration of ERT acquisition at a specific horizon is required [14]. The coverage of subsurface information given from electrical resistivity measurement depends on the space between the electrodes inserted into the soil for the measurements [193]. The spatial distribution of SM can be presented as 2D, 3D, or 4D tomograms [201]. ERT can also provide simultaneous data acquired from different depths and locations in order to improve the 4D spatiotemporal variability of SM [193]. Besides SM, the application of ERT for the assessment of RWU is also highlighted by numerous studies in order to monitor the impact of different irrigation schemes [202] and the extent of plant roots [14,203].

SM measurements by the EMI method are typically based on the strong relationship between the soil water distribution and ECa [204]. Different agricultural treatments like fertilizer applications might result in a complex relationship between SM and ECa [205]. EMI was initially used for soil salinity assessment before expanding to various applications [195]. In saline soil, soluble salt is the major physicochemical property influencing the apparent soil electrical conductivity; therefore, the interpretation is often straightforward [172]. In an area with a low salt concentration, ECa is mostly highly affected by SM variations [196,206,207].

Another method used to estimate SM is a GPR. SM is the dominant factor affecting the wave attenuation and velocity of GPR's electromagnetic signal, thus influencing the soil dielectric constant [199]. GPR has a disadvantage compared to ERT, as its performance decreases in electrically conductive media like fine-textured soil such as clay [14]. The GPR-derived soil dielectric constant can then be converted to volumetric SM using a technique called Topp's empirical relationship [208]. In the past decade, the development of multichannel GPR measurement became promising for SM observation [200]. This could allow the user to obtain a high-resolution measurement of the reflector depth and SM with less effort. Nowadays, the combination of GPR and EMI in an integrated inverse modeling scheme to obtain multi-layered media has been widely adopted, as shown by Mogadhas et al. [204] and Barca et al. [196].

Table 4. Various geophysical methods to characterize the soil water availability and dynamic in the vadose zone.

Geophysical Methods	Applications	References
ERT	Deliniation of soil facies	[162,163]
	SOM investigation	[166]
	Soil compaction assessment	[164]
	Monitoring SM variabilities	[14,163,191–193]
	RWU characterization for monitoring the impact of different irrigation schemes	[202]
	RWU characterization to assess the extent of root plant	[14,203]
EMI	Clay layer investigation	[175–177]
	Soil compaction assessment	[179,180]
	Monitoring SM variabilities	[196,197,206]
GPR	Soil structure monitoring	[183–185]
	Soil compaction assessment	[186,187]
	Monitoring SM variabilities	[196,199,200,209,210]
Seismic	Soil compaction assessment	[189,190]

5. Irrigation Modellings to Support Precision Agriculture

During the past decade, the domain of agricultural modeling has progressively evolved. Instead of focusing solely on the increase in farm productivity, agricultural modeling has expanded its application to recent challenges such as greenhouse gas emissions, food and water security, climate change mitigation, and carbon sequestration [211]. From the context of precision agriculture, agricultural modeling would overcome the insufficient on-farm dataset required in space and time to enhance farm management decisions. In general, crop yield, soil, the availability of natural resources, and the effects of human practices are the necessary information to understand the complex behaviour of an agricultural system [212]. Based on Jones et al. [212], the spatiotemporal scope of agricultural modeling varies depending on the problems that are being addressed by farmers, researchers, or decision-makers. It is widely known that the larger the scale, the more demanding the required data [213]. A brief overview of various applications of agricultural modeling is provided in Table 5.

Coupled Hydrologic–Crop Modelling

The rising concern for water and food security has elevated the need for coupled hydrological and crop-growth modeling [214]. Hydrological simulation refers to the numerical representation of soil water distribution in the soil-plant-atmosphere continuum. Most hydrological models are based on the Richards equation and the convection–dispersion equation in order to simulate water flow and solute movement in granular media [215]. Various hydrological models with different characteristics have been developed for this purpose, including SUTRA [216] TOUGH [217], UNSAT-1 [218], UNSAT-2 [219], SATURN [220], 3DFEMWATER [221], SVAT [222,223], SWAP [224,225], SWAT [226,227], and HYDRUS [215,228,229]. Among them, HYDRUS is the most frequently used model to simulate 1D, 2D and 3D hydrological movement in the unsaturated and saturated zones. According to Arnold et al. [230], six essential parameters should be considered and implemented in order to build a reliable hydrological model: computation efficiency, high spatial resolution, data input availability, continuity, the ability to simulate land-management scenarios, and the ability to provide reasonable results.

Crop growth models are mainly employed to simulate biophysical processes and to predict crop yield, which is affected by soil, weather, crop varieties, and cultivation practices, including irrigation and fertilizer application [231–233]. Commonly, crop growth is simulated based on mathematical expressions that describe the flow and conversion processes of water, nitrogen, and carbon [234]. Numerous models based on various concepts and underlying theories have been developed and successfully utilized over the years, such as DAISY [235,236], DSSAT [234,237], DSSAT-CERES [238,239], SUCROS [240], and WOFOST [241,242]. In addition, the integration of hydrological and crop growth models with other parameters, such as remote sensing data, could provide the improved, real-time calibration of model parameters [36].

The coupling of hydrological and crop modeling under spatial and temporal variations is essential in complex agricultural systems, despite being at an early stage of development [214]. Without the coupling of the two models, the accuracy of the crop growth might be decreased due to the oversimplification of the processes involved [243]. Recently, this approach was proposed by Mc Nider et al. [244], Pauwels et al. [231], Sheila et al. [234], Vaghefi et al. [245], Zhang et al. [243], and Zhou et al. [246]. Several challenges can surface during the process of coupling two models, such as the model simulation and application, methodology, and model hypothesis [243]. In order to select the appropriate methodology, a lot of factors should be considered, such as the scale, basin characteristics, availability of the dataset, method requirements, time constraints, and required accuracy [214].

Table 5. Overview of different applications of hydrologic, crop, and coupled models for agricultural practices.

Models		Applications	References
Hydrologic	Crop		
HYDRUS 1D	-	Nitrate accumulation and leaching simulation	[247]
HYDRUS 2D	-	Soil and plant water simulation under different irrigation systems	[228]
SWAT	-	The effect of climate change on hydrology and crop yield simulation	[226]
SWAT	-	Simulation of streamflow, total suspended nutrient, and sediment	[227]
SWAP	-	Field water cycle simulation under deficit irrigation	[224]
-	DSSAT	Simulation of crop yield under practice of conservation agriculture	[237]
-	DSSAT	Simulation of crop response to fertilizer microdosing	[239]
WaSSI	GidDSSAT	Estimation the impact of irrigation withdrawal on hydrologic flow	[244]
HYDRUS 1D	DSSAT	Soil water dynamic, crop growth and yield simulation	[234]
JULES	SUCROS	Dynamic crop growth simulation	[240]
SVAT	DAISY	Simulation of crop production and nitrate leaching	[236]
VIC	EPIC	Improvement discharge, SM and evapotranspiration simulation	[243]
HYDRUS 1D	WOFOST	Optimizing irrigation water and predicting crop yield	[246]
SWAT	MODSIM	Crop water productivity simulation	[245]

6. Precision Agriculture and Future Challenges concerning Proper Irrigation

Optical (Vis, NIR, SWIR), thermal, active, and passive microwave remote sensing have been proven to be viable approaches to support precision irrigation, from the local to the global scale. Despite providing high-resolution images, the ability of optical satellite acquisition is constrained by atmospheric conditions and solar illumination. Microwave remote sensing has the potential to complement the conventional remote sensing technique in irrigation monitoring. The primary advantage of microwave remote sensing is the ability to penetrate clouds, and that it can be acquired at any time (day and night). However, the characterization of vegetation properties due to irrigation practices and obtaining radar observation for a range of system configurations is still a challenging issue [141]. Even though each sensor (optical, microwave, and thermal) has its own limitation in agricultural monitoring, they are complementary to each other; thus, they can be integrated together for better results. Among remote sensing technologies, UAV might also offer low-cost

alternatives for agricultural monitoring, especially for small farms where the resolution is large enough to observe the variabilities of the soil and plant properties.

The lack of quantitative subsurface soil spatial data is known to be a major constraint for the development of hydrological models. This gap can be overcome by the utilization of geophysics-based measurement. The geophysical survey offers soil characterization in the vadose zone in a rapid, reliable, and cost-effective way. This approach offers spatially extensive and high-resolution information that helps the user to understand complex pictures of hydrological states and fluxes in the subsoil. The non-uniqueness of the signal response that results in misleading interpretation and uncertainty are some challenges that should be addressed for future studies. The high resolution of ERT acquisition is still restricted to a shallow depth due to the requirement of electrode spacing increments, limiting its potential for larger surveys [248]. On the other hand, despite its mobility, the vertical resolution of soil characterization acquired by EMI is low in many studies, and can be improved by applying new EMI instruments with multiple coil separations and orientations [173]. Combining various geophysical techniques might reduce the ambiguity of interpretation and improve the resolution [156].

In addition, agricultural modeling would overcome the insufficient on-farm dataset required in space and time to enhance farm management. Water states and fluxes inside soil and irrigation water demand can be reflected by hydrological and crop models, respectively. The coupling of crop and hydrological models would improve the accuracy of the model, and could help the decision-maker to predict crop yields based on the irrigation input and scheme. The upscaling process from the field scale to the regional scale offers the better understanding required by decision-maker to manage valuable resources and optimize crop productivity. However, this process needs extensive information representing the physical, chemical, and biological heterogeneities of the study areas. Moreover, the scarcity of the ground-based datasets used for calibration could limit the accuracy of the model. The uncertainty could come not only from the data input but also from the modeling approach applied. Therefore, the chosen data input along with the modeling approach is a critical step to obtain the modeling objectives. The development of a simple generic model that can be applied at various scales and is easy to integrate with other datasets due to its flexibility would help the user, particularly in an agricultural study [249].

7. Conclusions

This paper aims to assist farmers or decision-makers in better understanding the potential of recent advances in agricultural studies in the optimization of irrigation water use. The tremendous progress of remote sensing, geophysics, and modeling applications in agricultural studies have established them as advanced techniques which complement each other. The integration of remote sensing, geophysical surveys, and agrohydrological modeling will probably become a standard approach in agricultural practice in the future. Their applications to monitor variables in the soil-plant-atmosphere continuum include, but are not limited to, the soil texture, soil structure, soil compaction, SM, RWU, ET, crop chlorophyll, LAI, and VWC. The regular monitoring of these variables is necessary for the improvement of irrigation water use efficiency and the projection of the end-of-season crop yield as part of precision agriculture.

At the decision level, the delineation of the farm zone based on information retrieved from remote sensing, geophysics, and modeling could help farmers to manage valuable resources and optimize crop productivity by supplying the actual water requirement needed by the soil and plant [210,250]. Future advancements are expected to improve data processing techniques and reduce the acquisition cost; thus, the more significant benefits of remote sensing, geophysics and modeling for agricultural applications can be achieved. As the concept of precision agriculture is directly linked to the spatial and temporal variabilities of soil and plant properties, understanding these parameters would provide a solid foundation for farm development in order to achieve the ultimate goal of optimal agricultural management.

Author Contributions: Conceptualization, P.S.; formal analysis, A.P., P.S. and N.K.; writing—original draft preparation, A.P., P.S., N.K., M.D., Z.D., M.M., M.A. and P.K.; writing—review and editing, A.P., P.S., N.K., M.D., Z.D., M.M., M.A., B.T. and P.K.; supervision, P.S., N.K., M.A. and B.T.; project administration, P.S. and M.Y. All authors have read and agreed to the published version of the manuscript.

Funding: This research received no external funding.

Institutional Review Board Statement: Not applicable.

Informed Consent Statement: Not applicable.

Data Availability Statement: Not applicable.

Acknowledgments: The authors would like to acknowledge the support provided from the College of Petroleum Engineering and Geosciences and the Interdisciplinary Research Center for Membranes and Water Security, King Fahd University of Petroleum and Minerals, Saudi Arabia.

Conflicts of Interest: The authors declare no conflict of interest. The funders had no role in the design of the study; in the collection, analyses, or interpretation of data; in the writing of the manuscript, or in the decision to publish the results.

References

1. Siebert, S.; Döll, P. Quantifying blue and green virtual water contents in global crop production as well as potential production losses without irrigation. *J. Hydrol.* **2010**, *384*, 198–217. [\[CrossRef\]](#)
2. Siebert, S.; Burke, J.; Faures, J.M.; Frenken, K.; Hoogeveen, J.; Döll, P.; Portmann, F.T. Groundwater use for irrigation—A global inventory. *Hydrol. Earth Syst. Sci.* **2010**, *14*, 1863–1880. [\[CrossRef\]](#)
3. Chartzoulakis, K.; Bertaki, M. Sustainable Water Management in Agriculture under Climate Change. *Agric. Agric. Sci. Procedia* **2015**, *4*, 88–98. [\[CrossRef\]](#)
4. Leng, G.; Huang, M.; Tang, Q.; Leung, L.R. A modeling study of irrigation effects on global surface water and groundwater resources under a changing climate. *J. Adv. Model. Earth Syst.* **2015**, *7*, 1285–1304. [\[CrossRef\]](#)
5. Voss, K.A.; Famiglietti, J.S.; Lo, M.; de Linage, C.; Rodell, M.; Swenson, S.C. Groundwater depletion in the Middle East from GRACE with implications for transboundary water management in the Tigris-Euphrates-Western Iran region. *Water Resour. Res.* **2013**, *49*, 904–914. [\[CrossRef\]](#)
6. Richey, A.S.; Thomas, B.F.; Lo, M.H.; Reager, J.T.; Famiglietti, J.S.; Voss, K.; Swenson, S.; Rodell, M. Quantifying renewable groundwater stress with GRACE. *Water Resour. Res.* **2015**, *51*, 5217–5237. [\[CrossRef\]](#) [\[PubMed\]](#)
7. Döll, P.; Müller Schmied, H.; Schuh, C.; Portmann, F.T.; Eicker, A. Global-scale assessment of groundwater depletion and related groundwater abstractions: Combining hydrological modeling with information from well observations and GRACE satellites. *Water Resour. Res.* **2014**, *50*, 5698–5720. [\[CrossRef\]](#)
8. Zhang, J.; Guan, K.; Peng, B.; Pan, M.; Zhou, W.; Jiang, C.; Kimm, H.; Franz, T.E.; Grant, R.F.; Yang, Y.; et al. Sustainable irrigation based on co-regulation of soil water supply and atmospheric evaporative demand. *Nat. Commun.* **2021**, *12*, 5549. [\[CrossRef\]](#)
9. Gebbers, R.; Adamchuk, V.I. Precision agriculture and food security. *Science* **2010**, *327*, 828–831. [\[CrossRef\]](#)
10. Neupane, J.; Guo, W. Agronomic Basis and Strategies for Precision Water Management: A Review. *Agronomy* **2019**, *9*, 87. [\[CrossRef\]](#)
11. Calera, A.; Campos, I.; Osann, A.; D’Urso, G.; Menenti, M. Remote Sensing for Crop Water Management: From ET Modelling to Services for the End Users. *Sensors* **2017**, *17*, 1104. [\[CrossRef\]](#)
12. Evans, R.G.; Sadler, E.J. Methods and technologies to improve efficiency of water use. *Water Resour. Res.* **2008**, *44*, W00E04. [\[CrossRef\]](#)
13. Mauser, W.; Schädlich, S. Modelling the spatial distribution of evapotranspiration on different scales using remote sensing data. *J. Hydrol.* **1998**, *212–213*, 250–267. [\[CrossRef\]](#)
14. Garré, S.; Javaux, M.; Vanderborght, J.; Pagès, L.; Vereecken, H. Three-Dimensional Electrical Resistivity Tomography to Monitor Root Zone Water Dynamics. *Vadose Zone J.* **2011**, *10*, 412–424. [\[CrossRef\]](#)
15. Schymanski, S.J.; Sivapalan, M.; Roderick, M.L.; Beringer, J.; Hutley, L.B. An optimality-based model of the coupled soil moisture and root dynamics. *Hydrol. Earth Syst. Sci.* **2008**, *12*, 913–932. [\[CrossRef\]](#)
16. Vereecken, H.; Huisman, J.A.; Bogaen, H.; Vanderborght, J.; Vrugt, J.A.; Hopmans, J.W. On the value of soil moisture measurements in vadose zone hydrology: A review. *Water Resour. Res.* **2008**, *44*, W00D06. [\[CrossRef\]](#)
17. Babaeian, E.; Sadeghi, M.; Jones, S.B.; Montzka, C.; Vereecken, H.; Tuller, M. Ground, Proximal, and Satellite Remote Sensing of Soil Moisture. *Rev. Geophys.* **2019**, *57*, 530–616. [\[CrossRef\]](#)
18. Simyrdanis, K.; Tsourlos, P.; Soupios, P.; Tsokas, G.; Kim, J.-H.; Papadopoulos, N. Surface-to-tunnel electrical resistance tomography measurements. *Near Surf. Geophys.* **2015**, *13*, 343–354. [\[CrossRef\]](#)
19. Power, C.; Gerhard, J.I.; Tsourlos, P.; Soupios, P.; Simyrdanis, K.; Karaoulis, M. Improved time-lapse electrical resistivity tomography monitoring of dense non-aqueous phase liquids with surface-to-horizontal borehole arrays. *J. Appl. Geophys.* **2015**, *112*, 1–13. [\[CrossRef\]](#)

20. Stampolidis, A.; Soupios, P.; Vallianatos, F.; Tsokas, G.N. Detection of leaks in buried plastic water distribution pipes in urban places—A case study. In Proceedings of the 2nd International Workshop on Advanced Ground Penetrating Radar, Delft, The Netherlands, 14–16 May 2003; International Research Centre for Telecommunications-Transmission & Radar: Delft, The Netherlands, 2003; pp. 120–124.
21. Haboudane, D.; Miller, J.R.; Tremblay, N.; Zarco-Tejada, P.J.; Dextraze, L. Integrated narrow-band vegetation indices for prediction of crop chlorophyll content for application to precision agriculture. *Remote Sens. Environ.* **2002**, *81*, 416–426. [[CrossRef](#)]
22. Yamashita, H.; Sonobe, R.; Hirono, Y.; Morita, A.; Ikka, T. Dissection of hyperspectral reflectance to estimate nitrogen and chlorophyll contents in tea leaves based on machine learning algorithms. *Sci. Rep.* **2020**, *10*, 17360. [[CrossRef](#)] [[PubMed](#)]
23. Parry, C.; Blonquist, J.M.; Bugbee, B. In situ measurement of leaf chlorophyll concentration: Analysis of the optical/absolute relationship. *Plant Cell Environ.* **2014**, *37*, 2508–2520. [[CrossRef](#)]
24. Elarab, M.; Ticlavilca, A.M.; Torres-Rua, A.F.; Maslova, I.; McKee, M. Estimating chlorophyll with thermal and broadband multispectral high resolution imagery from an unmanned aerial system using relevance vector machines for precision agriculture. *Int. J. Appl. Earth Obs. Geoinf.* **2015**, *43*, 32–42. [[CrossRef](#)]
25. Gago, J.; Douthe, C.; Coopman, R.E.; Gallego, P.P.; Ribas-Carbo, M.; Flexas, J.; Escalona, J.; Medrano, H. UAVs challenge to assess water stress for sustainable agriculture. *Agric. Water Manag.* **2015**, *153*, 9–19. [[CrossRef](#)]
26. Hosikian, A.; Lim, S.; Halim, R.; Danquah, M.K. Chlorophyll Extraction from Microalgae: A Review on the Process Engineering Aspects. *Int. J. Chem. Eng.* **2010**, *2010*, 391632. [[CrossRef](#)]
27. Gitelson, A.A.; Viña, A.; Ciganda, V.; Rundquist, D.C.; Arkebauer, T.J. Remote estimation of canopy chlorophyll content in crops. *Geophys. Res. Lett.* **2005**, *32*, 403. [[CrossRef](#)]
28. Sims, D.A.; Gamon, J.A. Relationships between leaf pigment content and spectral reflectance across a wide range of species, leaf structures and developmental stages. *Remote Sens. Environ.* **2002**, *81*, 337–354. [[CrossRef](#)]
29. Delegido, J.; Alonso, L.; González, G.; Moreno, J. Estimating chlorophyll content of crops from hyperspectral data using a normalized area over reflectance curve (NAOC). *Int. J. Appl. Earth Obs. Geoinf.* **2010**, *12*, 165–174. [[CrossRef](#)]
30. Clevers, J.G.P.W.; Kooistra, L.; van den Brande, M.M.M. Using Sentinel-2 data for retrieving LAI and leaf and canopy chlorophyll content of a potato crop. *Remote Sens.* **2017**, *9*, 405. [[CrossRef](#)]
31. Prudnikova, E.; Savin, I.; Vindeker, G.; Grubina, P.; Shishkonakova, E.; Sharychev, D. Influence of soil background on spectral reflectance of winter wheat crop canopy. *Remote Sens.* **2019**, *11*, 1932. [[CrossRef](#)]
32. Simic Milas, A.; Romanko, M.; Reil, P.; Abeysinghe, T.; Marambe, A. The importance of leaf area index in mapping chlorophyll content of corn under different agricultural treatments using UAV images. *Int. J. Remote Sens.* **2018**, *39*, 5415–5431. [[CrossRef](#)]
33. Cowling, S.A.; Field, C.B. Environmental control of leaf area production: Implications for vegetation and land-surface modeling. *Global Biogeochem. Cycles* **2003**, *17*, 7-1–7-14. [[CrossRef](#)]
34. Liu, K.; Zhou, Q.B.; Wu, W.B.; Xia, T.; Tang, H.J. Estimating the crop leaf area index using hyperspectral remote sensing. *J. Integr. Agric.* **2016**, *15*, 475–491. [[CrossRef](#)]
35. Zheng, G.; Moskal, L.M. Retrieving Leaf Area Index (LAI) Using Remote Sensing: Theories, Methods and Sensors. *Sensors* **2009**, *9*, 2719–2745. [[CrossRef](#)] [[PubMed](#)]
36. Doraiswamy, P.C.; Hatfield, J.L.; Jackson, T.J.; Akhmedov, B.; Prueger, J.; Stern, A. Crop condition and yield simulations using Landsat and MODIS. *Remote Sens. Environ.* **2004**, *92*, 548–559. [[CrossRef](#)]
37. Son, N.T.; Chen, C.F.; Chen, C.R.; Chang, L.Y.; Duc, H.N.; Nguyen, L.D. Prediction of rice crop yield using MODIS EVI-LAI data in the Mekong Delta, Vietnam. *Int. J. Remote Sens.* **2013**, *34*, 7275–7292. [[CrossRef](#)]
38. Das, J.; Cross, G.; Qu, C.; Makineni, A.; Tokekar, P.; Mulgaonkar, Y.; Kumar, V. Devices, systems, and methods for automated monitoring enabling precision agriculture. In Proceedings of the IEEE International Conference on Automation Science and Engineering, Gothenburg, Sweden, 24–28 August 2015.
39. Hunt, E.R.; Li, L.; Yilmaz, M.T.; Jackson, T.J. Comparison of vegetation water contents derived from shortwave-infrared and passive-microwave sensors over central Iowa. *Remote Sens. Environ.* **2011**, *115*, 2376–2383. [[CrossRef](#)]
40. Xu, C.; Qu, J.J.; Hao, X.; Cosh, M.H.; Zhu, Z.; Gutenberg, L. Monitoring crop water content for corn and soybean fields through data fusion of MODIS and Landsat measurements in Iowa. *Agric. Water Manag.* **2020**, *227*, 105844. [[CrossRef](#)]
41. Alexakis, D.D.; Sarris, A.; Kalaitzidis, C.; Papadopoulos, N.; Soupios, P. Integrated use of satellite remote sensing, GIS, and ground spectroscopy techniques for monitoring olive oil mill waste disposal areas on the island of Crete, Greece. *Int. J. Remote Sens.* **2016**, *37*, 669–693. [[CrossRef](#)]
42. Jensen, J.R. *Remote Sensing of the Environment: An Earth Resource Perspective*, 2nd ed.; Pearson Education Limited: Essex, UK, 2014; Volume 1, ISBN 9780131889507.
43. Zhang, K.; Kimball, J.S.; Running, S.W. A review of remote sensing based actual evapotranspiration estimation. *Wiley Interdiscip. Rev. Water* **2016**, *3*, 834–853. [[CrossRef](#)]
44. Liou, Y.A.; Kar, S.K. Evapotranspiration estimation with remote sensing and various surface energy balance algorithms—a review. *Energies* **2014**, *7*, 2821–2849. [[CrossRef](#)]
45. Su, Z. The Surface Energy Balance System (SEBS) for estimation of turbulent heat fluxes. *Hydrol. Earth Syst. Sci.* **2002**, *6*, 85–100. [[CrossRef](#)]
46. Senay, G.B.; Budde, M.; Verdin, J.P.; Melesse, A.M. A coupled remote sensing and simplified surface energy balance approach to estimate actual evapotranspiration from irrigated fields. *Sensors* **2007**, *7*, 979–1000. [[CrossRef](#)]

47. Li, Z.L.; Tang, R.; Wan, Z.; Bi, Y.; Zhou, C.; Tang, B.; Yan, G.; Zhang, X. A review of current methodologies for regional Evapotranspiration estimation from remotely sensed data. *Sensors* **2009**, *9*, 3801–3853. [[CrossRef](#)] [[PubMed](#)]
48. Bastiaanssen, W.G.M.; Menenti, M.; Feddes, R.A.; Holtslag, A.A.M. A remote sensing surface energy balance algorithm for land (SEBAL). 1. Formulation. *J. Hydrol.* **1998**, *212–213*, 198–212. [[CrossRef](#)]
49. Allen, R.G.; Tasumi, M.; Morse, A.; Trezza, R.; Wright, J.L.; Bastiaanssen, W.; Kramber, W.; Lorite, I.; Robison, C.W. Satellite-Based Energy Balance for Mapping Evapotranspiration with Internalized Calibration (METRIC)—Applications. *J. Irrig. Drain. Eng.* **2007**, *133*, 395–406. [[CrossRef](#)]
50. Mallick, K.; Boegh, E.; Trebs, I.; Alfieri, J.G.; Kustas, W.P.; Prueger, J.H.; Niyogi, D.; Das, N.; Drewry, D.T.; Hoffmann, L.; et al. Reintroducing radiometric surface temperature into the Penman-Monteith formulation. *Water Resour. Res.* **2015**, *51*, 6214–6243. [[CrossRef](#)]
51. Norman, J.M.; Kustas, W.P.; Humes, K.S. Source approach for estimating soil and vegetation energy fluxes in observations of directional radiometric surface temperature. *Agric. For. Meteorol.* **1995**, *77*, 263–293. [[CrossRef](#)]
52. Colaizzi, P.D.; Kustas, W.P.; Anderson, M.C.; Agam, N.; Tolk, J.A.; Evett, S.R.; Howell, T.A.; Gowda, P.H.; O’Shaughnessy, S.A. Two-source energy balance model estimates of evapotranspiration using component and composite surface temperatures. *Adv. Water Resour.* **2012**, *50*, 134–151. [[CrossRef](#)]
53. Mecikalski, J.R.; Diak, G.R.; Anderson, M.C.; Norman, J.M. Estimating fluxes on continental scales using remotely sensed data in an atmospheric-land exchange model. *J. Appl. Meteorol.* **1999**, *38*, 1352–1369. [[CrossRef](#)]
54. Norman, J.M.; Anderson, M.C.; Kustas, W.P.; French, A.N.; Mecikalski, J.; Torn, R.; Diak, G.R.; Schmugge, T.J.; Tanner, B.C.W. Remote sensing of surface energy fluxes at 101-m pixel resolutions. *Water Resour. Res.* **2003**, *39*, 1221. [[CrossRef](#)]
55. Boulet, G.; Mougnot, B.; Lhomme, J.P.; Fanise, P.; Lili-Chabaane, Z.; Oliosio, A.; Bahir, M.; Rivalland, V.; Jarlan, L.; Merlin, O.; et al. The SPARSE model for the prediction of water stress and evapotranspiration components from thermal infra-red data and its evaluation over irrigated and rainfed wheat. *Hydrol. Earth Syst. Sci.* **2015**, *19*, 4653–4672. [[CrossRef](#)]
56. Burchard-Levine, V.; Nieto, H.; Riaño, D.; Migliavacca, M.; El-Madany, T.S.; Perez-Priego, O.; Carrara, A.; Martín, M.P. Seasonal adaptation of the thermal-based two-source energy balance model for estimating evapotranspiration in a semiarid tree-grass ecosystem. *Remote Sens.* **2020**, *12*, 904. [[CrossRef](#)]
57. Tang, R.; Li, Z.L. An End-Member-Based Two-Source Approach for Estimating Land Surface Evapotranspiration from Remote Sensing Data. *IEEE Trans. Geosci. Remote Sens.* **2017**, *55*, 5818–5832. [[CrossRef](#)]
58. Tang, Q.; Peterson, S.; Cuenca, R.H.; Hagimoto, Y.; Lettenmaier, D.P. Satellite-based near-real-time estimation of irrigated crop water consumption. *J. Geophys. Res. Atmos.* **2009**, *114*, D05114. [[CrossRef](#)]
59. Rwasoka, D.T.; Gumindoga, W.; Gwenzi, J. Estimation of actual evapotranspiration using the Surface Energy Balance System (SEBS) algorithm in the Upper Manyame catchment in Zimbabwe. *Phys. Chem. Earth* **2011**, *36*, 736–746. [[CrossRef](#)]
60. Senkondo, W.; Munishi, S.E.; Tumbo, M.; Nobert, J.; Lyon, S.W. Comparing remotely-sensed surface energy balance evapotranspiration estimates in heterogeneous and data-limited regions: A case study of Tanzania’s Kilombero Valley. *Remote Sens.* **2019**, *11*, 1289. [[CrossRef](#)]
61. Tasumi, M. Estimating evapotranspiration using METRIC model and Landsat data for better understandings of regional hydrology in the western Urmia Lake Basin. *Agric. Water Manag.* **2019**, *226*, 105805. [[CrossRef](#)]
62. Lian, J.; Huang, M. Comparison of three remote sensing based models to estimate evapotranspiration in an oasis-desert region. *Agric. Water Manag.* **2016**, *165*, 153–162. [[CrossRef](#)]
63. Bastiaanssen, W.G.M.; Cheema, M.J.M.; Immerzeel, W.W.; Miltenburg, I.J.; Pelgrum, H. Surface energy balance and actual evapotranspiration of the transboundary Indus Basin estimated from satellite measurements and the ETLook model. *Water Resour. Res.* **2012**, *48*, W11512. [[CrossRef](#)]
64. Mostafa, J.; Ali, B.; Mohsen, G.; Masoud, T. METRIC and WaPOR Estimates of Evapotranspiration over the Lake Urmia Basin: Comparative Analysis and Composite Assessment. *Water* **2019**, *11*, 1647.
65. Minacapilli, M.; Consoli, S.; Vanella, D.; Ciruolo, G.; Motisi, A. A time domain triangle method approach to estimate actual evapotranspiration: Application in a Mediterranean region using MODIS and MSG-SEVIRI products. *Remote Sens. Environ.* **2016**, *174*, 10–23. [[CrossRef](#)]
66. Carlson, T. An overview of the “triangle method” for estimating surface evapotranspiration and soil moisture from satellite imagery. *Sensors* **2007**, *7*, 1612–1629. [[CrossRef](#)]
67. Zhu, W.; Jia, S.; Lv, A. A Universal Ts-VI Triangle Method for the Continuous Retrieval of Evaporative Fraction from MODIS Products. *J. Geophys. Res. Atmos.* **2017**, *122*, 10206–10227. [[CrossRef](#)]
68. Li, B.; Cui, Y.; Geng, X.; Li, H. Improving the evapotranspiration estimation under cloudy condition by extending the Ts-VI triangle model. *Remote Sens.* **2021**, *13*, 1516. [[CrossRef](#)]
69. Cui, Y.; Ma, S.; Yao, Z.; Chen, X.; Luo, Z.; Fan, W.; Hong, Y. Developing a gap-filling algorithm using DNN for the Ts-VI triangle model to obtain temporally continuous daily actual evapotranspiration in an arid area of China. *Remote Sens.* **2020**, *12*, 1121. [[CrossRef](#)]
70. Rodell, M.; Famiglietti, J.S.; Chen, J.; Seneviratne, S.I.; Viterbo, P.; Holl, S.; Wilson, C.R. Basin scale estimates of evapotranspiration using GRACE and other observations. *Geophys. Res. Lett.* **2004**, *31*, 10–13. [[CrossRef](#)]
71. Ramillien, G.; Frappart, F.; Güntner, A.; Ngo-Duc, T.; Cazenave, A.; Laval, K. Time variations of the regional evapotranspiration rate from Gravity Recovery and Climate Experiment (GRACE) satellite gravimetry. *Water Resour. Res.* **2006**, *42*, W10403. [[CrossRef](#)]
72. Long, D.; Longuevergne, L.; Scanlon, B.R. Uncertainty in evapotranspiration from land surface modeling, remote sensing, and GRACE satellites. *Water Resour. Res.* **2014**, *50*, 1131–1151. [[CrossRef](#)]

73. Wan, Z.; Zhang, K.; Xue, X.; Hong, Z.; Hong, Y.; Gourley, J.J. Water balance-based actual evapotranspiration reconstruction from ground and satellite observations over the conterminous United States. *Water Resour. Res.* **2015**, *51*, 6485–6499. [[CrossRef](#)]
74. Yin, W.; Hu, L.; Zhang, M.; Wang, J.; Han, S.C. Statistical Downscaling of GRACE-Derived Groundwater Storage Using ET Data in the North China Plain. *J. Geophys. Res. Atmos.* **2018**, *123*, 5973–5987. [[CrossRef](#)]
75. Ghaderi, A.; Dasineh, M.; Shokri, M.; Abraham, J. Estimation of actual evapotranspiration using the remote sensing method and sebal algorithm: A case study in ein khosh plain, iran. *Hydrology* **2020**, *7*, 36. [[CrossRef](#)]
76. Bhattarai, N.; Mallick, K.; Brunsell, N.A.; Sun, G.; Jain, M. Regional evapotranspiration from an image-based implementation of the Surface Temperature Initiated Closure (STIC1.2) model and its validation across an aridity gradient in the conterminous US. *Hydrol. Earth Syst. Sci.* **2018**, *22*, 2311–2341. [[CrossRef](#)]
77. Diarra, A.; Jarlan, L.; Er-Raki, S.; Le Page, M.; Aouade, G.; Tavernier, A.; Boulet, G.; Ezzahar, J.; Merlin, O.; Khabba, S. Performance of the two-source energy budget (TSEB) model for the monitoring of evapotranspiration over irrigated annual crops in North Africa. *Agric. Water Manag.* **2017**, *193*, 71–88. [[CrossRef](#)]
78. Delogu, E.; Boulet, G.; Olioso, A.; Garrigues, S.; Brut, A.; Tallec, T.; Demarty, J.; Soudani, K.; Lagouarde, J.-P. Evaluation of the SPARSE Dual-Source Model for Predicting Water Stress and Evapotranspiration from Thermal Infrared Data over Multiple Crops and Climates. *Remote Sens.* **2018**, *10*, 1806. [[CrossRef](#)]
79. Tian, J.; Su, H.; Sun, X.; Chen, S.; He, H.; Zhao, L. Impact of the spatial domain size on the performance of the ts-vi triangle method in terrestrial evapotranspiration estimation. *Remote Sens.* **2013**, *5*, 1998–2013. [[CrossRef](#)]
80. Pan, Y.; Zhang, C.; Gong, H.; Yeh, P.J.F.; Shen, Y.; Guo, Y.; Huang, Z.; Li, X. Detection of human-induced evapotranspiration using GRACE satellite observations in the Haihe River basin of China. *Geophys. Res. Lett.* **2017**, *44*, 190–199. [[CrossRef](#)]
81. Hain, C.R.; Crow, W.T.; Mecikalski, J.R.; Anderson, M.C.; Holmes, T. An intercomparison of available soil moisture estimates from thermal infrared and passive microwave remote sensing and land surface modeling. *J. Geophys. Res. Atmos.* **2011**, *116*, D15107. [[CrossRef](#)]
82. Engman, E.T. Applications of microwave remote sensing of soil moisture for water resources and agriculture. *Remote Sens. Environ.* **1991**, *35*, 213–226. [[CrossRef](#)]
83. Yan, R.; Bai, J. A New Approach for Soil Moisture Downscaling in the Presence of Seasonal Difference. *Remote Sens. Environ.* **2020**, *12*, 2818. [[CrossRef](#)]
84. Chan, S.K.; Bindlish, R.; O’Neill, P.E.; Njoku, E.; Jackson, T.; Colliander, A.; Chen, F.; Burgin, M.; Dunbar, S.; Piepmeier, J.; et al. Assessment of the SMAP Passive Soil Moisture Product. *IEEE Trans. Geosci. Remote Sens.* **2016**, *54*, 4994–5007. [[CrossRef](#)]
85. Kerr, Y.H.; Al-Yaari, A.; Rodriguez-Fernandez, N.; Parrens, M.; Molero, B.; Leroux, D.; Bircher, S.; Mahmoodi, A.; Mialon, A.; Richaume, P.; et al. Overview of SMOS performance in terms of global soil moisture monitoring after six years in operation. *Remote Sens. Environ.* **2016**, *180*, 40–63. [[CrossRef](#)]
86. Ma, H.; Zeng, J.; Chen, N.; Zhang, X.; Cosh, M.H.; Wang, W. Satellite surface soil moisture from SMAP, SMOS, AMSR2 and ESA CCI: A comprehensive assessment using global ground-based observations. *Remote Sens. Environ.* **2019**, *231*, 111215. [[CrossRef](#)]
87. Kumar, S.V.; Peters-Lidard, C.D.; Santanello, J.A.; Reichle, R.H.; Draper, C.S.; Koster, R.D.; Nearing, G.; Jasinski, M.F. Evaluating the utility of satellite soil moisture retrievals over irrigated areas and the ability of land data assimilation methods to correct for unmodeled processes. *Hydrol. Earth Syst. Sci.* **2015**, *19*, 4463–4478. [[CrossRef](#)]
88. Lawston, P.M.; Santanello, J.A.; Kumar, S.V. Irrigation Signals Detected From SMAP Soil Moisture Retrievals. *Geophys. Res. Lett.* **2017**, *44*, 11860–11867. [[CrossRef](#)]
89. Brocca, L.; Tarpanelli, A.; Filippucci, P.; Dorigo, W.; Zaussinger, F.; Gruber, A.; Fernández-Prieto, D. How much water is used for irrigation? A new approach exploiting coarse resolution satellite soil moisture products. *Int. J. Appl. Earth Obs. Geoinf.* **2018**, *73*, 752–766. [[CrossRef](#)]
90. Jalilvand, E.; Tajrishy, M.; Ghazi Zadeh Hashemi, S.A.; Brocca, L. Quantification of irrigation water using remote sensing of soil moisture in a semi-arid region. *Remote Sens. Environ.* **2019**, *231*, 111226. [[CrossRef](#)]
91. Zappa, L.; Schläffer, S.; Bauer-Marschallinger, B.; Nendel, C.; Zimmerman, B.; Dorigo, W. Detection and quantification of irrigation water amounts at 500 m using sentinel-1 surface soil moisture. *Remote Sens.* **2021**, *13*, 1727. [[CrossRef](#)]
92. Zaussinger, F.; Dorigo, W.; Gruber, A.; Tarpanelli, A.; Filippucci, P.; Brocca, L. Estimating irrigation water use over the contiguous United States by combining satellite and reanalysis soil moisture data. *Hydrol. Earth Syst. Sci.* **2019**, *23*, 897–923. [[CrossRef](#)]
93. Alexakis, D.D.; Mexis, F.D.K.; Vozinaki, A.E.K.; Daliakopoulos, I.N.; Tsanis, I.K. Soil moisture content estimation based on Sentinel-1 and auxiliary earth observation products. A hydrological approach. *Sensors* **2017**, *17*, 1455. [[CrossRef](#)] [[PubMed](#)]
94. Xing, M.; He, B.; Ni, X.; Wang, J.; An, G.; Shang, J.; Huang, X. Retrieving surface soil moisture over wheat and soybean fields during growing season using modified water cloud model from RADARSAT-2 SAR data. *Remote Sens.* **2019**, *11*, 1956. [[CrossRef](#)]
95. Zribi, M.; Muddu, S.; Bousbih, S.; Al Bitar, A.; Tomer, S.K.; Baghdadi, N.; Bandyopadhyay, S. Analysis of L-band SAR data for soil moisture estimations over agricultural areas in the tropics. *Remote Sens.* **2019**, *11*, 1122. [[CrossRef](#)]
96. Gorraeb, A.; Zribi, M.; Baghdadi, N.; Mougenot, B.; Fanise, P.; Chabaane, Z.L. Retrieval of both soil moisture and texture using TerraSAR-X images. *Remote Sens.* **2015**, *7*, 10098–10116. [[CrossRef](#)]
97. Njoku, E.G.; Entekhabi, D. Passive microwave remote sensing of soil moisture. *J. Hydrol.* **1996**, *184*, 101–129. [[CrossRef](#)]
98. Barrett, B.W.; Dwyer, E.; Whelan, P. Soil moisture retrieval from active spaceborne microwave observations: An evaluation of current techniques. *Remote Sens.* **2009**, *1*, 210–242. [[CrossRef](#)]
99. Sonkar, I.; Kotnoor, H.P.; Sen, S. Estimation of root water uptake and soil hydraulic parameters from root zone soil moisture and deep percolation. *Agric. Water Manag.* **2019**, *222*, 38–47. [[CrossRef](#)]

100. Pablos, M.; González-Zamora, Á.; Sánchez, N.; Martínez-Fernández, J. Assessment of root zone soil moisture estimations from SMAP, SMOS and MODIS observations. *Remote Sens.* **2018**, *10*, 981. [[CrossRef](#)]
101. Ford, T.W.; Harris, E.; Quiring, S.M. Estimating root zone soil moisture using near-surface observations from SMOS. *Hydrol. Earth Syst. Sci.* **2014**, *18*, 139–154. [[CrossRef](#)]
102. Dumedah, G.; Walker, J.P.; Merlin, O. Root-zone soil moisture estimation from assimilation of downscaled Soil Moisture and Ocean Salinity data. *Adv. Water Resour.* **2015**, *84*, 14–22. [[CrossRef](#)]
103. Baldwin, D.; Manfreda, S.; Keller, K.; Smithwick, E.A.H. Predicting root zone soil moisture with soil properties and satellite near-surface moisture data across the conterminous United States. *J. Hydrol.* **2017**, *546*, 393–404. [[CrossRef](#)]
104. Owe, M.; de Jeu, R.; Holmes, T. Multisensor historical climatology of satellite-derived global land surface moisture. *J. Geophys. Res. Earth Surf.* **2008**, *113*, F01002. [[CrossRef](#)]
105. Zhang, X.; Zhang, T.; Zhou, P.; Shao, Y.; Gao, S. Validation analysis of SMAP and AMSR2 soil moisture products over the United States using ground-based measurements. *Remote Sens.* **2017**, *9*, 104. [[CrossRef](#)]
106. Liu, J.; Chai, L.; Lu, Z.; Liu, S.; Qu, Y.; Geng, D.; Song, Y.; Guan, Y.; Guo, Z.; Wang, J.; et al. Evaluation of SMAP, SMOS-IC, FY3B, JAXA, and LPRM Soil moisture products over the Qinghai-Tibet Plateau and Its surrounding areas. *Remote Sens.* **2019**, *11*, 792. [[CrossRef](#)]
107. Cui, C.; Xu, J.; Zeng, J.; Chen, K.S.; Bai, X.; Lu, H.; Chen, Q.; Zhao, T. Soil moisture mapping from satellites: An intercomparison of SMAP, SMOS, FY3B, AMSR2, and ESA CCI over two dense network regions at different spatial scales. *Remote Sens.* **2018**, *10*, 33. [[CrossRef](#)]
108. Wu, S.; Ren, J.; Chen, Z.; Yang, P.; Li, H. Soil moisture estimation based on the microwave scattering mechanism during different crop phenological periods in a winter wheat-producing region. *J. Hydrol.* **2020**, *590*, 125521. [[CrossRef](#)]
109. Sandholt, I.; Rasmussen, K.; Andersen, J. A simple interpretation of the surface temperature/vegetation index space for assessment of surface moisture status. *Remote Sens. Environ.* **2002**, *79*, 213–224. [[CrossRef](#)]
110. Zhang, D.; Zhou, G. Estimation of soil moisture from optical and thermal remote sensing: A review. *Sensors* **2016**, *16*, 1308. [[CrossRef](#)] [[PubMed](#)]
111. Rahimzadeh-Bajgiran, P.; Berg, A.A.; Champagne, C.; Omasa, K. Estimation of soil moisture using optical/thermal infrared remote sensing in the Canadian Prairies. *ISPRS J. Photogramm. Remote Sens.* **2013**, *83*, 94–103. [[CrossRef](#)]
112. Zhang, D.; Tang, R.; Zhao, W.; Tang, B.; Wu, H.; Shao, K.; Li, Z.L. Surface soil water content estimation from thermal remote sensing based on the temporal variation of land surface temperature. *Remote Sens.* **2014**, *6*, 3170–3187. [[CrossRef](#)]
113. Xu, T.; Guo, Z.; Xia, Y.; Ferreira, V.G.; Liu, S.; Wang, K.; Yao, Y.; Zhang, X.; Zhao, C. Evaluation of twelve evapotranspiration products from machine learning, remote sensing and land surface models over conterminous United States. *J. Hydrol.* **2019**, *578*, 124105. [[CrossRef](#)]
114. Sadeghi, M.; Babaeian, E.; Tuller, M.; Jones, S.B. The optical trapezoid model: A novel approach to remote sensing of soil moisture applied to Sentinel-2 and Landsat-8 observations. *Remote Sens. Environ.* **2017**, *198*, 52–68. [[CrossRef](#)]
115. Wu, K.; Rodriguez, G.A.; Zajc, M.; Jacquemin, E.; Clément, M.; De Coster, A.; Lambot, S. A new drone-borne GPR for soil moisture mapping. *Remote Sens. Environ.* **2019**, *235*, 111456. [[CrossRef](#)]
116. Wang, S.; Garcia, M.; Ibrom, A.; Jakobsen, J.; Köppl, C.J.; Mallick, K.; Looms, M.C.; Bauer-Gottwein, P. Mapping root-zone soil moisture using a temperature-vegetation triangle approach with an unmanned aerial system: Incorporating surface roughness from structure from motion. *Remote Sens.* **2018**, *10*, 1978. [[CrossRef](#)]
117. Casas-Mulet, R.; Pander, J.; Ryu, D.; Stewardson, M.J.; Geist, J. Unmanned Aerial Vehicle (UAV)-Based Thermal Infra-Red (TIR) and Optical Imagery Reveals Multi-Spatial Scale Controls of Cold-Water Areas Over a Groundwater-Dominated Riverscape. *Front. Environ. Sci.* **2020**, *8*, 64. [[CrossRef](#)]
118. Kim, S.; Liu, Y.Y.; Johnson, F.M.; Parinussa, R.M.; Sharma, A. Remote Sensing of Environment a global comparison of alternate AMSR2 soil moisture products: Why do they differ? *Remote Sens. Environ.* **2015**, *161*, 43–62. [[CrossRef](#)]
119. Bousbih, S.; Zribi, M.; Hajj, M.E.; Baghdadi, N.; Lili-Chabaane, Z.; Gao, Q.; Fanise, P. Soil moisture and irrigation mapping in a semi-arid region, based on the synergetic use of Sentinel-1 and Sentinel-2 data. *Remote Sens.* **2018**, *10*, 1953. [[CrossRef](#)]
120. Singh Rawat, K.; Kumar Singh, S.; Kumar Pal, R. Synergetic methodology for estimation of soil moisture over agricultural area using Landsat-8 and Sentinel-1 satellite data. *Remote Sens. Appl. Soc. Environ.* **2019**, *15*, 100250. [[CrossRef](#)]
121. Haboudane, D.; Miller, J.R.; Pattey, E.; Zarco-Tejada, P.J.; Strachan, I.B. Hyperspectral vegetation indices and novel algorithms for predicting green LAI of crop canopies: Modeling and validation in the context of precision agriculture. *Remote Sens. Environ.* **2004**, *90*, 337–352. [[CrossRef](#)]
122. Kanning, M.; Kühling, I.; Trautz, D.; Jarmer, T. High-resolution UAV-based hyperspectral imagery for LAI and chlorophyll estimations from wheat for yield prediction. *Remote Sens.* **2018**, *10*, 2000. [[CrossRef](#)]
123. Croft, H.; Chen, J.M.; Zhang, Y. The applicability of empirical vegetation indices for determining leaf chlorophyll content over different leaf and canopy structures. *Ecol. Complex.* **2014**, *17*, 119–130. [[CrossRef](#)]
124. Darvishzadeh, R.; Skidmore, A.; Schlerf, M.; Atzberger, C. Inversion of a radiative transfer model for estimating vegetation LAI and chlorophyll in a heterogeneous grassland. *Remote Sens. Environ.* **2008**, *112*, 2592–2604. [[CrossRef](#)]
125. Houborg, R.; Boegh, E. Mapping leaf chlorophyll and leaf area index using inverse and forward canopy reflectance modeling and SPOT reflectance data. *Remote Sens. Environ.* **2008**, *112*, 186–202. [[CrossRef](#)]
126. Meroni, M.; Colombo, R.; Panigada, C. Inversion of a radiative transfer model with hyperspectral observations for LAI mapping in poplar plantations. *Remote Sens. Environ.* **2004**, *92*, 195–206. [[CrossRef](#)]

127. Colombo, R.; Bellingeri, D.; Fasolini, D.; Marino, C.M. Retrieval of leaf area index in different vegetation types using high resolution satellite data. *Remote Sens. Environ.* **2003**, *86*, 120–131. [[CrossRef](#)]
128. Gamon, J.A.; Surfus, J.S. Assessing leaf pigment content and activity with a reflectometer. *New Phytol.* **1999**, *143*, 105–117. [[CrossRef](#)]
129. Towers, P.C.; Strever, A.; Poblete-Echeverría, C. Comparison of vegetation indices for leaf area index estimation in vertical shoot positioned vine canopies with and without grenbiule hail-protection netting. *Remote Sens.* **2019**, *11*, 1073. [[CrossRef](#)]
130. Gong, P.; Pu, R.; Biging, G.S.; Larrieu, M.R. Estimation of forest leaf area index using vegetation indices derived from Hyperion hyperspectral data. *IEEE Trans. Geosci. Remote Sens.* **2003**, *41*, 1355–1362. [[CrossRef](#)]
131. Gitelson, A.A.; Gritz, Y.; Merzlyak, M.N. Relationships between leaf chlorophyll content and spectral reflectance and algorithms for non-destructive chlorophyll assessment in higher plant leaves. *J. Plant Physiol.* **2003**, *160*, 271–282. [[CrossRef](#)]
132. Daughtry, C.S.T.; Walthall, C.L.; Kim, M.S.; De Colstoun, E.B.; McMurtrey, J.E. Estimating corn leaf chlorophyll concentration from leaf and canopy reflectance. *Remote Sens. Environ.* **2000**, *74*, 229–239. [[CrossRef](#)]
133. Zhang, F.; Zhou, G. Estimation of vegetation water content using hyperspectral vegetation indices: A comparison of crop water indicators in response to water stress treatments for summer maize. *BMC Ecol.* **2019**, *19*, 18. [[CrossRef](#)] [[PubMed](#)]
134. Ullah, S.; Skidmore, A.K.; Ramoelo, A.; Groen, T.A.; Naeem, M.; Ali, A. Retrieval of leaf water content spanning the visible to thermal infrared spectra. *ISPRS J. Photogramm. Remote Sens.* **2014**, *93*, 56–64. [[CrossRef](#)]
135. Jin, X.; Shi, C.; Yu, C.Y.; Yamada, T.; Sacks, E.J. Determination of leaf water content by visible and near-infrared spectrometry and multivariate calibration in *Miscanthus*. *Front. Plant Sci.* **2017**, *8*, 721. [[CrossRef](#)] [[PubMed](#)]
136. Ceccato, P.; Flasse, S.; Tarantola, S.; Jacquemoud, S.; Grégoire, J.M. Detecting vegetation leaf water content using reflectance in the optical domain. *Remote Sens. Environ.* **2001**, *77*, 22–33. [[CrossRef](#)]
137. Quemada, C.; Pérez-Escudero, J.M.; Gonzalo, R.; Ederra, I.; Santesteban, L.G.; Torres, N.; Iriarte, J.C. Remote sensing for plant water content monitoring: A review. *Remote Sens.* **2021**, *13*, 2088. [[CrossRef](#)]
138. Huang, J.; Chen, D.; Cosh, M.H. Sub-pixel reflectance unmixing in estimating vegetation water content and dry biomass of corn and soybeans cropland using normalized difference water index (NDWI) from satellites. *Int. J. Remote Sens.* **2009**, *30*, 2075–2104. [[CrossRef](#)]
139. Chen, D.; Huang, J.; Jackson, T.J. Vegetation water content estimation for corn and soybeans using spectral indices derived from MODIS near- and short-wave infrared bands. *Remote Sens. Environ.* **2005**, *98*, 225–236. [[CrossRef](#)]
140. Kim, Y.; Van Zyl, J.J. A time-series approach to estimate soil moisture using polarimetric radar data. *IEEE Trans. Geosci. Remote Sens.* **2009**, *47*, 2519–2527. [[CrossRef](#)]
141. Kim, Y.; Jackson, T.; Bindlish, R.; Lee, H.; Hong, S. Radar vegetation index for estimating the vegetation water content of rice and soybean. *IEEE Geosci. Remote Sens. Lett.* **2012**, *9*, 564–568. [[CrossRef](#)]
142. Huang, Y.; Walker, J.P.; Gao, Y.; Wu, X.; Monerris, A. Estimation of Vegetation Water Content from the Radar Vegetation Index at L-Band. *IEEE Trans. Geosci. Remote Sens.* **2016**, *54*, 981–989. [[CrossRef](#)]
143. Ma, J.; Huang, S.; Li, J.; Li, X.; Song, X.; Leng, P.; Sun, Y. Estimating Vegetation Water Content of Corn and Soybean Using Different Polarization Ratios Based on L-and S-Band Radar Data. *IEEE Geosci. Remote Sens. Lett.* **2017**, *14*, 364–368. [[CrossRef](#)]
144. Szigarski, C.; Jagdhuber, T.; Baur, M.; Thiel, C.; Parrons, M.; Wigneron, J.P.; Piles, M.; Entekhabi, D. Analysis of the Radar Vegetation Index and potential improvements. *Remote Sens.* **2018**, *10*, 1776. [[CrossRef](#)]
145. Chang, J.G.; Shoshany, M.; Oh, Y. Polarimetric Radar Vegetation Index for Biomass Estimation in Desert Fringe Ecosystems. *IEEE Trans. Geosci. Remote Sens.* **2018**, *56*, 7102–7108. [[CrossRef](#)]
146. Mandal, D.; Kumar, V.; Ratha, D.; Dey, S.; Bhattacharya, A.; Lopez-Sanchez, J.M.; McNairn, H.; Rao, Y.S. Dual polarimetric radar vegetation index for crop growth monitoring using sentinel-1 SAR data. *Remote Sens. Environ.* **2020**, *247*, 111954. [[CrossRef](#)]
147. Gerber, F.; Marion, R.; Olioso, A.; Jacquemoud, S.; Ribeiro da Luz, B.; Fabre, S. Modeling directional-hemispherical reflectance and transmittance of fresh and dry leaves from 0.4 μ m to 5.7 μ m with the PROSPECT-VISIR model. *Remote Sens. Environ.* **2011**, *115*, 404–414. [[CrossRef](#)]
148. Xue, J.; Su, B. Significant remote sensing vegetation indices: A review of developments and applications. *J. Sensors* **2017**, *2017*, 1353691. [[CrossRef](#)]
149. Neinavaz, E.; Schlerf, M.; Darvishzadeh, R.; Gerhards, M.; Skidmore, A.K. Thermal infrared remote sensing of vegetation: Current status and perspectives. *Int. J. Appl. Earth Obs. Geoinf.* **2021**, *102*, 102415. [[CrossRef](#)]
150. Carmona, F.; Rivas, R.; Fonnegra, D.C. Vegetation index to estimate chlorophyll content from multispectral remote sensing data. *Eur. J. Remote Sens.* **2015**, *48*, 319–326. [[CrossRef](#)]
151. Roosjen, P.P.J.; Brede, B.; Suomalainen, J.M.; Bartholomeus, H.M.; Kooistra, L.; Clevers, J.G.P.W. Improved estimation of leaf area index and leaf chlorophyll content of a potato crop using multi-angle spectral data—potential of unmanned aerial vehicle imagery. *Int. J. Appl. Earth Obs. Geoinf.* **2018**, *66*, 14–26. [[CrossRef](#)]
152. Pan, H.; Chen, Z.; Ren, J.; Li, H.; Wu, S. Modeling Winter Wheat Leaf Area Index and Canopy Water Content with Three Different Approaches Using Sentinel-2 Multispectral Instrument Data. *IEEE J. Sel. Top. Appl. Earth Obs. Remote Sens.* **2019**, *12*, 482–492. [[CrossRef](#)]
153. Yilmaz, M.T.; Hunt, E.R.; Jackson, T.J. Remote sensing of vegetation water content from equivalent water thickness using satellite imagery. *Remote Sens. Environ.* **2008**, *112*, 2514–2522. [[CrossRef](#)]
154. Tabbagh, A.; Dabas, M.; Hesse, A.; Panissod, C.P. Soil resistivity: A non-invasive tool to map soil structure horizonation. *Geoderma* **2000**, *97*, 393–404. [[CrossRef](#)]
155. Allred, B.J.; Ehsani, M.R.; Daniels, J.J. General considerations for geophysical methods applied to agriculture. In *Handbook of Agricultural Geophysics*; CRC Press: Boca Raton, FL, USA, 2008.

156. Romero-Ruiz, A.; Linde, N.; Keller, T.; Or, D. A Review of Geophysical Methods for Soil Structure Characterization. *Rev. Geophys.* **2018**, *56*, 672–697. [[CrossRef](#)]
157. Besson, A.; Cousin, I.; Samouëlian, A.; Boizard, H.; Richard, G. Structural heterogeneity of the soil tilled layer as characterized by 2D electrical resistivity surveying. *Soil Tillage Res.* **2004**, *79*, 239–249. [[CrossRef](#)]
158. Ranjy Roodposhti, H.; Hafizi, M.K.; Soleymani Kermani, M.R.; Ghorbani Nik, M.R. Electrical resistivity method for water content and compaction evaluation, a laboratory test on construction material. *J. Appl. Geophys.* **2019**, *168*, 49–58. [[CrossRef](#)]
159. Keller, T.; Carizzoni, M.; Berisso, F.E.; Stettler, M.; Lamandé, M. Measuring the Dynamic Soil Response during Repeated Wheeling Using Seismic Methods. *Vadose Zone J.* **2013**, *12*, vzt2013.01.0033. [[CrossRef](#)]
160. Ntarlagiannis, D.; Robinson, J.; Soupios, P.; Slater, L. Field-scale electrical geophysics over an olive oil mill waste deposition site: Evaluating the information content of resistivity versus induced polarization (IP) images for delineating the spatial extent of organic contamination. *J. Appl. Geophys.* **2016**, *135*, 418–426. [[CrossRef](#)]
161. Kowalczyk, S.; Maślakowski, M.; Tucholka, P. Determination of the correlation between the electrical resistivity of non-cohesive soils and the degree of compaction. *J. Appl. Geophys.* **2014**, *110*, 43–50. [[CrossRef](#)]
162. Chrétien, M.; Lataste, J.F.; Fabre, R.; Denis, A. Electrical resistivity tomography to understand clay behavior during seasonal water content variations. *Eng. Geol.* **2014**, *169*, 112–123. [[CrossRef](#)]
163. Nielson, T.; Bradford, J.; Pierce, J.; Seyfried, M. Soil structure and soil moisture dynamics inferred from time-lapse electrical resistivity tomography. *Catena* **2021**, *207*, 105553. [[CrossRef](#)]
164. Keller, T.; Colombi, T.; Ruiz, S.; Manalili, M.P.; Rek, J.; Stadelmann, V.; Wunderli, H.; Breitenstein, D.; Reiser, R.; Oberholzer, H.; et al. Long-Term Soil Structure Observatory for Monitoring Post-Compaction Evolution of Soil Structure. *Vadose Zone J.* **2017**, *16*, vzt2016.11.0118. [[CrossRef](#)]
165. Cheng, Q.; Tao, M.; Chen, X.; Binley, A. Evaluation of electrical resistivity tomography (ERT) for mapping the soil–rock interface in karstic environments. *Environ. Earth Sci.* **2019**, *78*, 439. [[CrossRef](#)]
166. Turki, N.; Elaoud, A.; Gabtni, H.; Trabelsi, I.; Khalfallah, K.K. Agricultural soil characterization using 2D electrical resistivity tomography (ERT) after direct and intermittent digestate application. *Arab. J. Geosci.* **2019**, *12*, 423. [[CrossRef](#)]
167. Simyrdanis, K.; Papadopoulos, N.; Soupios, P.; Kirkou, S.; Tsourlos, P. Characterization and monitoring of subsurface contamination from Olive Oil Mills' waste waters using Electrical Resistivity Tomography. *Sci. Total Environ.* **2018**, 637–638, 991–1003. [[CrossRef](#)] [[PubMed](#)]
168. Kirmizakis, P.; Soupios, P.; Simyrdanis, K.; Kirkou, S.; Papadopoulos, N.; Tsourlos, P.; Ntarlagiannis, D.; Robinson, J.; Slater, L.; Kim, J.H. Geoelectrical characterization of an olive oil mill waste (OOMW) site. In Proceedings of the 28th Symposium on the Application of Geophysics to Engineering and Environmental Problems, Austin, TX, USA, 22–26 March 2015.
169. Rani, P.; Piegari, E.; Di Maio, R.; Vitagliano, E.; Soupios, P.; Milano, L. Monitoring time evolution of self-potential anomaly sources by a new global optimization approach. Application to organic contaminant transport. *J. Hydrol.* **2019**, *575*, 955–964. [[CrossRef](#)]
170. Kirmizakis, P.; Kalderis, D.; Ntarlagiannis, D.; Soupios, P. Preliminary assessment on the application of biochar and spectral-induced polarization for wastewater treatment. *Near Surf. Geophys.* **2020**, *18*, 109–122. [[CrossRef](#)]
171. Siddiq, M.O.; Tawabini, B.; Kirmizakis, P.; Kalderis, D.; Ntarlagiannis, D.; Soupios, P. Combining geophysics and material science for environmental remediation: Real-time monitoring of Fe-biochar arsenic wastewater treatment. *Chemosphere* **2021**, *284*, 131390. [[CrossRef](#)] [[PubMed](#)]
172. Corwin, D.L.; Lesch, S.M. Apparent soil electrical conductivity measurements in agriculture. *Comput. Electron. Agric.* **2005**, *46*, 11–43. [[CrossRef](#)]
173. Brogi, C.; Huisman, J.A.; Pätzold, S.; von Hebel, C.; Weihermüller, L.; Kaufmann, M.S.; van der Kruk, J.; Vereecken, H. Large-scale soil mapping using multi-configuration EMI and supervised image classification. *Geoderma* **2019**, *335*, 133–148. [[CrossRef](#)]
174. Martini, E.; Werban, U.; Zacharias, S.; Pohle, M.; Dietrich, P.; Wollschläger, U. Repeated electromagnetic induction measurements for mapping soil moisture at the field scale: Validation with data from a wireless soil moisture monitoring network. *Hydrol. Earth Syst. Sci.* **2017**, *21*, 495–513. [[CrossRef](#)]
175. Triantafyllis, J.; Lesch, S.M. Mapping clay content variation using electromagnetic induction techniques. *Comput. Electron. Agric.* **2005**, *46*, 203–237. [[CrossRef](#)]
176. Sudduth, K.A.; Kitchen, N.R.; Wiebold, W.J.; Batchelor, W.D.; Bollero, G.A.; Bullock, D.G.; Clay, D.E.; Palm, H.L.; Pierce, F.J.; Schuler, R.T.; et al. Relating apparent electrical conductivity to soil properties across the north-central USA. *Comput. Electron. Agric.* **2005**, *46*, 263–283. [[CrossRef](#)]
177. De Benedetto, D.; Castrignano, A.; Sollitto, D.; Modugno, F.; Buttafuoco, G.; Papa, G. Lo Integrating geophysical and geostatistical techniques to map the spatial variation of clay. *Geoderma* **2012**, 171–172, 53–63. [[CrossRef](#)]
178. Bronson, K.F.; Booker, J.D.; Officer, S.J.; Lascano, R.J.; Maas, S.J.; Searcy, S.W.; Booker, J. Apparent electrical conductivity, soil properties and spatial covariance in the U.S. Southern High Plains. *Precis. Agric.* **2005**, *6*, 297–311. [[CrossRef](#)]
179. Schmäck, J.; Weihermüller, L.; Klotzsche, A.; Hebel, C.; Pätzold, S.; Welp, G.; Vereecken, H. Large-scale detection and quantification of harmful soil compaction in a post-mining landscape using multi-configuration electromagnetic induction. *Soil Use Manag.* **2021**, *38*, 212–228. [[CrossRef](#)]
180. Al-Gaadi, K.A. Employing electromagnetic induction technique for the assessment of soil compaction. *Am. J. Agric. Biol. Sci.* **2012**, *7*, 425–434. [[CrossRef](#)]

181. André, F.; van Leeuwen, C.; Saussez, S.; Van Durmen, R.; Bogaert, P.; Moghadas, D.; de Rességuier, L.; Delvaux, B.; Vereecken, H.; Lambot, S. High-resolution imaging of a vineyard in south of France using ground-penetrating radar, electromagnetic induction and electrical resistivity tomography. *J. Appl. Geophys.* **2012**, *78*, 113–122. [[CrossRef](#)]
182. Zajíčová, K.; Chuman, T. Application of ground penetrating radar methods in soil studies: A review. *Geoderma* **2019**, *343*, 116–129. [[CrossRef](#)]
183. Lombardi, F.; Lualdi, M. Step-frequency ground penetrating radar for agricultural soil morphology characterisation. *Remote Sens.* **2019**, *11*, 1075. [[CrossRef](#)]
184. Zhang, J.; Lin, H.; Doolittle, J. Soil layering and preferential flow impacts on seasonal changes of GPR signals in two contrasting soils. *Geoderma* **2014**, *213*, 560–569. [[CrossRef](#)]
185. Novakova, E.; Karous, M.; Zajíček, A.; Karousova, M. Evaluation of ground penetrating radar and vertical electrical sounding methods to determine soil horizons and bedrock at the locality dehtaře. *Soil Water Res.* **2013**, *8*, 105–112. [[CrossRef](#)]
186. Wang, P.; Hu, Z.; Zhao, Y.; Li, X. Experimental study of soil compaction effects on GPR signals. *J. Appl. Geophys.* **2016**, *126*, 128–137. [[CrossRef](#)]
187. Akinsunmade, A.; Tomecka-Suchoń, S.; Pysz, P. Correlation between agrotechnical properties of selected soil types and corresponding GPR response. *Acta Geophys.* **2019**, *67*, 1913–1919. [[CrossRef](#)]
188. McAnallen, L.; Doherty, R.; Donohue, S.; Kirmizakis, P.; Mendonça, C. Combined use of geophysical and geochemical methods to assess areas of active, degrading and restored blanket bog. *Sci. Total Environ.* **2018**, *621*, 762–771. [[CrossRef](#)]
189. Donohue, S.; Forristal, D.; Donohue, L.A. Detection of soil compaction using seismic surface waves. *Soil Tillage Res.* **2013**, *128*, 54–60. [[CrossRef](#)]
190. Romero-Ruiz, A.; Linde, N.; Baron, L.; Solazzi, S.G.; Keller, T.; Or, D. Seismic signatures reveal persistence of soil compaction. *Vadose Zone J.* **2021**, *20*, e20140. [[CrossRef](#)]
191. Michot, D.; Benderitter, Y.; Dorigny, A.; Nicoullaud, B.; King, D.; Tabbagh, A. Spatial and temporal monitoring of soil water content with an irrigated corn crop cover using surface electrical resistivity tomography. *Water Resour. Res.* **2003**, *39*, 1138. [[CrossRef](#)]
192. Schwartz, B.F.; Schreiber, M.E.; Yan, T. Quantifying field-scale soil moisture using electrical resistivity imaging. *J. Hydrol.* **2008**, *362*, 234–246. [[CrossRef](#)]
193. Calamita, G.; Brocca, L.; Perrone, A.; Piscitelli, S.; Lapenna, V.; Melone, F.; Moramarco, T. Electrical resistivity and TDR methods for soil moisture estimation in central Italy test-sites. *J. Hydrol.* **2012**, *454–455*, 101–112. [[CrossRef](#)]
194. Chambers, J.E.; Gunn, D.A.; Wilkinson, P.B.; Meldrum, P.I.; Haslam, E.; Holyoake, S.; Kirkham, M.; Kuras, O.; Merritt, A.; Wragg, J. 4D electrical resistivity tomography monitoring of soil moisture dynamics in an operational railway embankment. *Near Surf. Geophys.* **2014**, *12*, 61–72. [[CrossRef](#)]
195. Doolittle, J.A.; Brevik, E.C. The use of electromagnetic induction techniques in soils studies. *Geoderma* **2014**, *223–225*, 33–45. [[CrossRef](#)]
196. Barca, E.; De Benedetto, D.; Stellacci, A.M. Contribution of EMI and GPR proximal sensing data in soil water content assessment by using linear mixed effects models and geostatistical approaches. *Geoderma* **2019**, *343*, 280–293. [[CrossRef](#)]
197. Moghadas, D.; Jadoon, K.Z.; McCabe, M.F. Spatiotemporal monitoring of soil moisture from EMI data using DCT-based Bayesian inference and neural network. *J. Appl. Geophys.* **2019**, *169*, 226–238. [[CrossRef](#)]
198. Lunt, I.A.; Hubbard, S.S.; Rubin, Y. Soil moisture content estimation using ground-penetrating radar reflection data. *J. Hydrol.* **2005**, *307*, 254–2697. [[CrossRef](#)]
199. Zhou, L.; Yu, D.; Wang, Z.; Wang, X. Soil water content estimation using high-frequency ground penetrating radar. *Water* **2019**, *11*, 1036. [[CrossRef](#)]
200. Klotzsche, A.; Jonard, F.; Looms, M.C.; van der Kruk, J.; Huisman, J.A. Measuring Soil Water Content with Ground Penetrating Radar: A Decade of Progress. *Vadose Zone J.* **2018**, *17*, 1–9. [[CrossRef](#)]
201. Loke, M.H.; Barker, R.D. Rapid least-squares inversion of apparent resistivity pseudosections by a quasi-Newton method. *Geophys. Prospect.* **1996**, *44*, 131–152. [[CrossRef](#)]
202. Vanella, D.; Cassiani, G.; Busato, L.; Boaga, J.; Barbagallo, S.; Binley, A.; Consoli, S. Use of small scale electrical resistivity tomography to identify soil-root interactions during deficit irrigation. *J. Hydrol.* **2018**, *556*, 310–324. [[CrossRef](#)]
203. Mary, B.; Vanella, D.; Consoli, S.; Cassiani, G. Assessing the extent of citrus trees root apparatus under deficit irrigation via multi-method geo-electrical imaging. *Sci. Rep.* **2019**, *9*, 9913. [[CrossRef](#)] [[PubMed](#)]
204. Moghadas, D.; André, F.; Slob, E.C.; Vereecken, H.; Lambot, S. Joint full-waveform analysis of off-ground zero-offset ground penetrating radar and electromagnetic induction synthetic data for estimating soil electrical properties. *Geophys. J. Int.* **2010**, *182*, 1267–1278. [[CrossRef](#)]
205. Altdorff, D.; Galagedara, L.; Nadeem, M.; Cheema, M.; Unc, A. Effect of agronomic treatments on the accuracy of soil moisture mapping by electromagnetic induction. *Catena* **2018**, *164*, 96–106. [[CrossRef](#)]
206. Brevik, E.C.; Fenton, T.E.; Lazari, A. Soil electrical conductivity as a function of soil water content and implications for soil mapping. *Precis. Agric.* **2006**, *7*, 393–404. [[CrossRef](#)]
207. Sherlock, M.D.; McDonnell, J.J. A new tool for hillslope hydrologists: Spatially distributed groundwater level and soilwater content measured using electromagnetic induction. *Hydrol. Process.* **2003**, *17*, 1965–1977. [[CrossRef](#)]
208. Topp, G.C.; Davis, J.L.; Annan, A.P. Electromagnetic Determination of Soil Water Content: Measurements in Coaxial Transmission Lines. *Water Resour. Res.* **1980**, *16*, 574–582. [[CrossRef](#)]

209. Jonard, F.; Mahmoudzadeh, M.; Roisin, C.; Weihermüller, L.; André, F.; Minet, J.; Vereecken, H.; Lambot, S. Characterization of tillage effects on the spatial variation of soil properties using ground-penetrating radar and electromagnetic induction. *Geoderma* **2013**, *207–208*, 310–322. [[CrossRef](#)]
210. Cavallo, G.; De Benedetto, D.; Castrignanò, A.; Quarto, R.; Vonella, A.V.; Buttafuoco, G. Use of geophysical data for assessing 3D soil variation in a durum wheat field and their association with crop yield. *Biosyst. Eng.* **2016**, *152*, 28–40. [[CrossRef](#)]
211. Holzworth, D.P.; Snow, V.; Janssen, S.; Athanasiadis, I.N.; Donatelli, M.; Hoogenboom, G.; White, J.W.; Thorburn, P. Agricultural production systems modelling and software: Current status and future prospects. *Environ. Model. Softw.* **2015**, *72*, 276–286. [[CrossRef](#)]
212. Jones, J.W.; Antle, J.M.; Basso, B.; Boote, K.J.; Conant, R.T.; Foster, I.; Godfray, H.C.J.; Herrero, M.; Howitt, R.E.; Janssen, S.; et al. Brief history of agricultural systems modeling. *Agric. Syst.* **2017**, *155*, 240–254. [[CrossRef](#)]
213. Vereecken, H.; Schnepf, A.; Hopmans, J.W.; Javaux, M.; Or, D.; Roose, T.; Vanderborght, J.; Young, M.H.; Amelung, W.; Aitkenhead, M.; et al. Modeling Soil Processes: Review, Key Challenges, and New Perspectives. *Vadose Zone J.* **2016**, *15*, 1–57. [[CrossRef](#)]
214. Siad, S.M.; Iacobellis, V.; Zdruli, P.; Gioia, A.; Stavi, I.; Hoogenboom, G. A review of coupled hydrologic and crop growth models. *Agric. Water Manag.* **2019**, *224*, 105746. [[CrossRef](#)]
215. Šimůnek, J.; Jarvis, N.J.; Van Genuchten, M.T.; Gärdenäs, A. Review and comparison of models for describing non-equilibrium and preferential flow and transport in the vadose zone. *J. Hydrol.* **2003**, *272*, 14–35. [[CrossRef](#)]
216. Voss, C. *A Finite-Element Simulation Model for Saturated-Unsaturated, Fluid-Density-Dependent Groundwater Flow with Energy Transport or Chemically-Reactive Single-Species Solute Transport*; U.S. Geological Survey: Panama City, FL, USA, 1984.
217. 'Pruess, K.; 'Tsang, Y.; 'Wang, J. Modeling of strongly heat driven flow in partially saturated fractured porous media. In Proceedings of the 17th International Congress of International Association of Hydrogeologists on Hydrogeology of Rocks of Low Permeability, Tucson, AZ, USA, 7–10 January 1985; University of California: Oakland, CA, USA, 1985.
218. Van Genuchten, M.T. A comparison of numerical solutions of the one-dimensional unsaturated-saturated flow and mass transport equations. *Adv. Water Resour.* **1982**, *5*, 47–55. [[CrossRef](#)]
219. Neuman, S.P.; Feddes, R.A.; Bresler, E. Finite Element Analysis of Two-Dimensional Flow in Soils Considering Water Uptake by Roots: I. Theory. *Proc. Soil Sci. Soc. Am.* **1975**, *39*, 224–230. [[CrossRef](#)]
220. Huyakorn, P.; Thomas, S.; Mercer, J.; Lester, B. *SATURN: A Finite Element Model for Simulating Saturated-Unsaturated Flow and Radioactive Radionuclide Transport*; Electric Power Research Institute: Palo Alto, CA, USA, 1983.
221. Yeh, G.T. *1DFEMWATER: A One-Dimensional Finite Element Model of WATER Flow through Saturated-Unsaturated Media*; Oak Ridge National Lab.: Oak Ridge, TN, USA, 1988.
222. Olioso, A.; Inoue, Y.; Ortega-Farias, S.; Demarty, J.; Wigneron, J.P.; Braud, I.; Jacob, F.; Lecharpentier, P.; Otlé, C.; Calvet, J.C.; et al. Future directions for advanced evapotranspiration modeling: Assimilation of remote sensing data into crop simulation models and SVAT models. *Irrig. Drain. Syst.* **2005**, *19*, 377–412. [[CrossRef](#)]
223. Petropoulos, G.; Carlson, T.N.; Wooster, M.J. An overview of the use of the SimSphere Soil Vegetation Atmosphere Transfer (SVAT) model for the study of land-atmosphere interactions. *Sensors* **2009**, *9*, 4286–4308. [[CrossRef](#)]
224. Ma, Y.; Feng, S.; Huo, Z.; Song, X. Application of the SWAP model to simulate the field water cycle under deficit irrigation in Beijing, China. *Math. Comput. Model.* **2011**, *54*, 1044–1052. [[CrossRef](#)]
225. Martínez-Ferri, E.; Muriel-Fernández, J.L.; Díaz, R.A.R. Soil water balance modelling using SWAP: An application for irrigation water management and climate change adaptation in citrus. *Outlook Agric.* **2013**, *42*, 93–102. [[CrossRef](#)]
226. Chen, Y.; Marek, G.W.; Marek, T.H.; Moorhead, J.E.; Heflin, K.R.; Brauer, D.K.; Gowda, P.H.; Srinivasan, R. Simulating the impacts of climate change on hydrology and crop production in the Northern High Plains of Texas using an improved SWAT model. *Agric. Water Manag.* **2019**, *221*, 13–24. [[CrossRef](#)]
227. Shrestha, M.K.; Recknagel, F.; Frizenschaf, J.; Meyer, W. Assessing SWAT models based on single and multi-site calibration for the simulation of flow and nutrient loads in the semi-arid Onkaparinga catchment in South Australia. *Agric. Water Manag.* **2016**, *175*, 61–71. [[CrossRef](#)]
228. Autovino, D.; Rallo, G.; Provenzano, G. Predicting soil and plant water status dynamic in olive orchards under different irrigation systems with Hydrus-2D: Model performance and scenario analysis. *Agric. Water Manag.* **2018**, *203*, 225–235. [[CrossRef](#)]
229. Ghazouani, H.; Rallo, G.; Mguidiche, A.; Latrech, B.; Douh, B.; Boujelben, A.; Provenzano, G. Assessing Hydrus-2D model to investigate the effects of different on-farm irrigation strategies on potato crop under subsurface drip irrigation. *Water* **2019**, *11*, 540. [[CrossRef](#)]
230. Arnold, J.G.; Srinivasan, R.; Mutiah, R.S.; Williams, J.R. Large area hydrologic modeling and assessment part I: Model development. *J. Am. Water Resour. Assoc.* **1998**, *34*, 73–89. [[CrossRef](#)]
231. Pauwels, V.R.N.; Verhoest, N.E.C.; De Lannoy, G.J.M.; Guissard, V.; Lucau, C.; Defourny, P. Optimization of a coupled hydrology-crop growth model through the assimilation of observed soil moisture and leaf area index values using an ensemble Kalman filter. *Water Resour. Res.* **2007**, *43*, 244–247. [[CrossRef](#)]
232. Huang, J.; Gómez-Dans, J.L.; Huang, H.; Ma, H.; Wu, Q.; Lewis, P.E.; Liang, S.; Chen, Z.; Xue, J.H.; Wu, Y.; et al. Assimilation of remote sensing into crop growth models: Current status and perspectives. *Agric. For. Meteorol.* **2019**, 276–277, 107609. [[CrossRef](#)]
233. Brogi, C.; Huisman, J.A.; Herbst, M.; Weihermüller, L.; Klosterhalfen, A.; Montzka, C.; Reichenau, T.G.; Vereecken, H. Simulation of spatial variability in crop leaf area index and yield using agroecosystem modeling and geophysics-based quantitative soil information. *Vadose Zone J.* **2020**, *19*, e20009. [[CrossRef](#)]

234. Shelia, V.; Šimunek, J.; Boote, K.; Hoogenboom, G. Coupling DSSAT and HYDRUS-1D for simulations of soil water dynamics in the soil-plant-atmosphere system. *J. Hydrol. Hydromech.* **2018**, *66*, 232–245. [[CrossRef](#)]
235. Abrahamsen, P.; Hansen, S. Daisy: An open soil-crop-atmosphere system model. *Environ. Model. Softw.* **2000**, *15*, 313–330. [[CrossRef](#)]
236. Manevski, K.; Børgesen, C.D.; Li, X.; Andersen, M.N.; Abrahamsen, P.; Hu, C.; Hansen, S. Integrated modelling of crop production and nitrate leaching with the Daisy model. *MethodsX* **2016**, *3*, 350–363. [[CrossRef](#)] [[PubMed](#)]
237. Corbeels, M.; Chirat, G.; Messad, S.; Thierfelder, C. Performance and sensitivity of the DSSAT crop growth model in simulating maize yield under conservation agriculture. *Eur. J. Agron.* **2016**, *76*, 41–53. [[CrossRef](#)]
238. Ma, L.; Hoogenboom, G.; Ahuja, L.R.; Ascough, J.C.; Saseendran, S.A. Evaluation of the RZWQM-CERES-maize hybrid model for maize production. *Agric. Syst.* **2006**, *87*, 274–295. [[CrossRef](#)]
239. Tovihoudji, P.G.; Akponikpè, P.B.I.; Agbossou, E.K.; Biolders, C.L. Using the DSSAT model to support decision making regarding fertilizer microdosing for maize production in the sub-humid region of Benin. *Front. Environ. Sci.* **2019**, *7*, 3. [[CrossRef](#)]
240. Van den Hoof, C.; Hanert, E.; Vidale, P.L. Simulating dynamic crop growth with an adapted land surface model-JULES-SUCROS: Model development and validation. *Agric. For. Meteorol.* **2011**, *151*, 137–153. [[CrossRef](#)]
241. Bai, T.; Zhang, N.; Chen, Y.; Mercatoris, B. Assessing the performance of the WOFOST model in simulating jujube fruit tree growth under different irrigation regimes. *Sustainability* **2019**, *11*, 1466. [[CrossRef](#)]
242. De Wit, A.; Boogaard, H.; Fumagalli, D.; Janssen, S.; Knapen, R.; van Kraalingen, D.; Supit, I.; van der Wijngaart, R.; van Diepen, K. 25 years of the WOFOST cropping systems model. *Agric. Syst.* **2019**, *168*, 154–167. [[CrossRef](#)]
243. Zhang, Y.; Wu, Z.; Singh, V.P.; He, H.; He, J.; Yin, H.; Zhang, Y. Coupled hydrology-crop growth model incorporating an improved evapotranspiration module. *Agric. Water Manag.* **2021**, *246*, 106691. [[CrossRef](#)]
244. McNider, R.T.; Handyside, C.; Doty, K.; Ellenburg, W.L.; Cruise, J.F.; Christy, J.R.; Moss, D.; Sharda, V.; Hoogenboom, G.; Caldwell, P. An integrated crop and hydrologic modeling system to estimate hydrologic impacts of crop irrigation demands. *Environ. Model. Softw.* **2015**, *72*, 341–355. [[CrossRef](#)]
245. Vaghefi, S.A.; Abbaspour, K.C.; Faramarzi, M.; Srinivasan, R.; Arnold, J.G. Modeling crop water productivity using a coupled SWAT-MODSIM model. *Water* **2017**, *9*, 157. [[CrossRef](#)]
246. Zhou, J.; Cheng, G.; Li, X.; Hu, B.X.; Wang, G. Numerical Modeling of Wheat Irrigation using Coupled HYDRUS and WOFOST Models. *Soil Sci. Soc. Am. J.* **2012**, *76*, 648–662. [[CrossRef](#)]
247. Colombani, N.; Mastrociccio, M.; Vincenzi, F.; Castaldelli, G. Modeling soil nitrate accumulation and leaching in conventional and conservation agriculture cropping systems. *Water* **2020**, *12*, 1571. [[CrossRef](#)]
248. Gourdol, L.; Clément, R.; Juilleret, J.; Pfister, L.; Hissler, C. Large-scale ERT surveys for investigating shallow regolith properties and architecture. *Hydrol. Earth Syst. Sci. Discuss.* **2018**, 1–39. [[CrossRef](#)]
249. Manivasagam, V.S.; Rozenstein, O. Practices for upscaling crop simulation models from field scale to large regions. *Comput. Electron. Agric.* **2020**, *175*, 105554. [[CrossRef](#)]
250. Peralta, N.R.; Costa, J.L. Delineation of management zones with soil apparent electrical conductivity to improve nutrient management. *Comput. Electron. Agric.* **2013**, *99*, 218–226. [[CrossRef](#)]